Coeval extensional shearing and lateral underflow during Late Cretaceous core complex development in the Niğde Massif, Central Anatolia, Turkey

Pierre Gautier, Erdin Bozkurt, Valérie Bosse, Erwan Hallot, Kadir Dirik

Coeval extensional shearing and lateral underflow during Late Cretaceous core complex development in the Niğde Massif, Central Anatolia, Turkey

Pierre Gautier[1], Erdin Bozkurt[2], Valérie Bosse[3], Erwan Hallot[1], and Kadir Dirik[2,4]

[1]Géosciences Rennes, UMR 6118 CNRS, Université Rennes 1, Rennes, France.

[2]Department of Geological Engineering, Tectonic Research Unit, Middle East Technical University, Ankara, Turkey.

[3]Laboratoire Magmas-Volcans, UMR 6524 CNRS, Université Blaise Pascal, Clermont-Ferrand, France.

[4]Department of Geological Engineering, Hacettepe University, Ankara, Turkey.

The Niğde Massif, at the southern tip of the Central Anatolian Crystalline Complex, consists of two structural units. Foliations in the lower unit define a dome cored by migmatites. The contact between the two units bears all the elements of a ductile to brittle extensional detachment. Hence the Niğde Massif represents an extensional metamorphic core complex. Top-to-NE/ENE shearing at higher levels of the lower unit relates to displacement along the detachment. Deeper levels of the lower unit display high-temperature top-to-SSW ductile shearing. The two shearing deformations show a difference in the mean trend of stretching lineations of up to 58°. New $^{40}Ar/^{39}Ar$ ages combined with previously published data enable us to infer that the two shears were contemporaneous. In our favored interpretation, oblique shearing in the core of the dome reflects lateral underflow, i.e., horizontal flowing of the lower crust in a direction highly oblique to the direction of extension. As a result of the interaction between lateral underflow and down-dip shearing along the overlying detachment, distinct structural domains are expected to exist within the migmatitic part of the core complex, with observed counterparts in the Niğde dome. Lateral underflow may reflect "inward" flow on the scale of the core complex. Regional-scale channel flow is an alternative that would better account for the record of non-coaxial deformation in the core of the dome. More generally, we suspect that the development of lateral underflow in a metamorphic core complex more likely reflects regional channel flow, rather than local inward flow.

1. Introduction

The accommodation of lithospheric extension in regions made up of a thick and hot continental crust, such as regions previously involved in an orogen, is a matter of ongoing debate, particularly the role and behavior of the lower crust during extension [e.g., *Lister and Davis,* 1989; *Wernicke,* 1990; *Buck,* 1991; *Brun et al.,* 1994; *McKenzie et al.,* 2000; *Tirel et al.,* 2004, 2006]. As a complement to analytical, numerical and experimental approaches, the study of natural examples is important for better understanding the key processes and establishing the conditions at which they occur. Among these natural examples, those exposing high-grade rocks exhumed from lower crustal levels are particularly informative [e.g., *Gautier et al.,* 1993; *Brun and Van den Driessche,* 1994; *Lagarde et al.,* 1994; *Amato and Miller,* 2004; *Teyssier et al.,* 2005]. In this paper, we analyse one such example in Central Anatolia.

The Central Anatolian Crystalline Complex (CACC) [*Göncüoğlu et al.,* 1991], also known as Kırşehir Massif [e.g., *Görür et al.,* 1984], is one of the largest metamorphic complexes in the Alpine orogen of the Eastern Mediterranean (Figure 1). To date, its evolution has been discussed mainly on the basis of relatively abundant petrological and geochemical data [e.g., *Göncüoğlu,* 1986; *Akıman et al.,* 1993; *Floyd et al.,* 2000; *Whitney et al.,* 2001, 2003; *Kadıoğlu et al.,* 2003; *Köksal et al.,* 2004; *Ilbeyli,* 2005], and in the light of tectono-stratigraphic constraints deduced from adjacent Late Cretaceous-Cenozoic sedimentary basins [e.g., *Görur et al.,* 1984; *Dirik et al.,* 1999; *Kaymakci,* 2000; *Clark and Robertson,* 2002]. In contrast, structural studies within the CACC remain scarce. Beneath a widespread cover of Neogene sediments and volcanics, much of the CACC exposes high-grade metamorphic rocks associated with abundant granitoids. The complex therefore has a typical high-temperature character [e.g., *Göncüoğlu,* 1986; *Akıman et al.,* 1993; *Whitney et al.,* 2001]. Geochronological data on these rocks cluster over a limited age range within the Late Cretaceous, documenting a short duration of the high-temperature event, followed by fast cooling [e.g., *Göncüoğlu,* 1986; *Whitney et al.,* 2003; *Köksal et al.,* 2004; *Ilbeyli,* 2005]. Clastic sediments accumulated at about the same time, both ontop and on the margins of the CACC [e.g., *Görur et al.,* 1984; *Dirik et al.,* 1999; *Clark and Robertson,* 2002]. These features, although not strictly diagnostic, strongly suggest that crustal extension played a significant role in the evolution of the complex, as already proposed by some authors [*Whitney and Dilek,* 1997; *Dirik et al.,* 1999; *Okay and Tüysüz,* 1999]. Thus, the CACC seems appropriate for an investigation of how extensional tectonics may develop in hot orogens, or in orogens that include a large high-grade core.

Here we present the results of a structural study carried out in the Niğde Massif, a metamorphic dome located at the southern tip of the CACC (Figure 1). Two main shearing events have been identified in the high-grade metamorphic series of the dome. Higher levels of the series have undergone ductile to brittle shearing along a NE/ENE-dipping extensional detachment which was briefly described in an earlier paper [*Gautier et al.,* 2002]. In contrast, the migmatitic core of the dome displays pronounced top-to-SSW ductile shearing. Together with radiometric data from the literature, new $^{40}Ar/^{39}Ar$ ages enable us to document that the two shearing events were contemporaneous. The significance of top-to-SSW shearing in the core of the dome is discussed in the light of these constraints. The Niğde dome likely represents an instance of core complex in which lateral underflow, i.e., horizontal flowing of the lower crust in a direction orthogonal or highly oblique to the direction of extension, has developed in response to highly localized extension in the middle and upper crust and/or high-magnitude extension on the regional scale. Such a situation has been rarely depicted in the literature [*MacCready et al.,* 1997; *Andronicos et al.,* 2003; *Amato and Miller,* 2004]. The Niğde dome is then used as an illustration for assessing the structural development of extensional domes cored by migmatitic rocks, and for discussing the dynamics of lower crustal flow during crustal extension. The consequences of this study for the establishment of a geodynamic scenario on the scale of the CACC will be the topic of a future paper.

2. Geological Setting

2.1. Metamorphic and Magmatic Rocks of the Niğde Massif

Much of the mountainous area corresponding to the Niğde Massif consists of high-grade metamorphic rocks of predominantly sedimentary origin (Figure 2). According to a synthetic log established by *Göncüoğlu et al.* [1991] [see also *Floyd et al.,* 2000], the lower part of the metamorphic series ("Gümüşler formation") is made of paragneisses with minor marbles and amphibolites; higher levels consist of a thinly bedded package of marbles, quartzites, micaschists and amphibolites ("Kaleboynu formation") overlain by a much thicker layer of marble with thin quartzite interbeds near its top ("Aşıgediği formation"). *Whitney and Dilek* [1998] estimated near-peak P-T conditions at around 5-6 kbar and >700°C in garnet-sillimanite paragneisses of the Gümüşler formation, the results of garnet-biotite thermometry suggesting temperatures in the range of 680-780°C. The superposition of Kaleboynu and Aşıgediği formations onto Gümüşler paragneisses is visible in the northwestern part of the massif, southeast of Gümüşler (Figures 2 and 3). In this area, the paragneisses commonly

display migmatitic textures. According to *Göncüoğlu et al.* [1991], two large slices of Gümüşler formation are also found further east and southeast (Figure 2). Along its western margin, the eastern slice overlies rocks of the Kaleboynu formation; near its southern end, the southeastern slice overlies the thick Aşıgediği marble layer (Figures 3 and 4). The dominantly metapelitic content of these slices supports their correlation with the underlying Gümüşler formation. Nevertheless, a difference in metamorphic grade is suggested by the fact that the paragneisses and micaschists in the eastern slice commonly show relictic migmatitic textures, while those in the southeastern slice usually lack signs of migmatization. In the southeastern slice, garnet micaschists and amphibolites have recorded temperature conditions of at least 630-650°C [*Whitney et al.,* 2001].

In addition to minor amphibolites in the Gümüşler and Kaleboynu formations, thicker bodies of basic and ultrabasic rocks occur higher in the rock pile. *Göncüoğlu et al.* [1991] describe these rocks as an ophiolite nappe emplaced ontop of the metamorphic series, usually separated from them by an olistostromic formation that carries blocks from both the ophiolite nappe and the underlying Aşıgediği formation. However, two distinct types of basic-ultrabasic rocks occur in the upper part of the Niğde rock pile [*Floyd et al.,* 2000; *Gautier et al.,* 2002]. To the south, such rocks are found as slices belonging to high levels of the high-grade metamorphic series. This is documented by the amphibolite facies deformation seen in most of the metabasites, showing a fabric paralleling that in underlying and overlying marbles and quartzites of the Aşıgediği formation. According to *Göncüoğlu et al.* [1991], these slices include both fragments of the ophiolite nappe and the underlying olistostromic formation, while *Floyd et al.* [2000] refer to them as a metamorphosed ophiolitic mélange. Along the northern and northeastern margins of the massif, large exposures of massive gabbro are found together with minor tonalitic intrusives (Figure 2). In contrast with the south, these rocks usually show pure magmatic textures and mineralogical assemblages. Some of the gabbros display a preferred mineral orientation (Figure 6a); this fabric is crosscut by tonalitic dikes having diffuse margins and either no fabric or a slight internal fabric paralleling their walls, which indicates that these fabrics are magmatic in origin. For *Whitney and Dilek* [1998], it is unclear whether these gabbros are in tectonic contact with the high-grade metamorphic rocks of the Niğde Massif, or intrude them. Where it can be seen, however, the contact is obviously tectonic, with the gabbros overlying the metamorphic rocks through a flat-lying fault zone [*Göncüoğlu et al.,* 1991] (Figures 3 and 4). In a thickness of about 10 m above the contact, the gabbros show greenschist facies deformation within decimeter- to meter-thick shear zones (Figure 6b). Significantly, small exposures of ultrabasic rocks are associated with the massive

gabbros [*Göncüoğlu et al.,* 1991], reinforcing the interpretation that these rocks form part of an ophiolite nappe. In agreement with this view, *Floyd et al.* [2000] have shown that the massive gabbros from the Niğde Massif bear the same geochemical signature as better exposed sections of a stratiform ophiolite found further north in the CACC. Importantly, the geochemical signature of the massive gabbros is distinct from that of the ophiolitic mélange within the high-grade metamorphic series. This led *Floyd et al.* [2000] to suggest the existence of two obduction nappes, and related thrust events, in the CACC. Irrespectively, this difference in geochemistry shows that an interpretation of the metamorphosed ophiolitic mélange as the immediate footwall of a single ophiolite nappe (represented by the massive gabbros), as initially proposed by *Göncüoğlu et al.* [1991], is too simplistic. In the Niğde Massif, the metamorphosed mélange and the massive gabbros are not in contact, supporting this view. More significantly, the massive gabbros have experienced limited post-magmatic deformation culminating in greenschist facies conditions [*Whitney and Dilek,* 1998; this work], whereas the metamorphic pile underneath, including the ophiolitic mélange, is characterized by the pervasive record of much higher temperature conditions (>700°C in the lower part of the pile, and at least 630°C in the southeastern slice of Gümüşler formation). This shows that two main structural units have to be considered in the Niğde Massif, with the upper one having experienced significantly lower peak conditions of metamorphism [*Gautier et al.,* 2002]. In the following, these two units are reported as the lower unit and the upper unit.

Granitoids are abundant in the Niğde Massif, intruding the high-grade metamorphic series. The main intrusion is the Üçkapılı granite [*Göncüoğlu,* 1986], exposed from the center of the massif to the northeast (Figure 2). Smaller exposures of granitoid, similar in appearance to the main body, are also widespread further northwest and south. The most common facies is a two-mica granite. Analyses on samples from several small intrusions in the northwest document that the magma was peraluminous, with a high initial Sr ratio (0.7104 ± 0.0009) [*Göncüoğlu,* 1986; *Akıman et al.,* 1993]. U-Pb geochronology on a sample from the main body shows that most zircons include an inherited core [*Whitney et al.,* 2003]. These features indicate that Üçkapılı-type magmas originate from partial melting of the continental crust [*Göncüoğlu,* 1986; *Whitney et al.,* 2003]. Pressure conditions during emplacement were probably around 3-4 kbar [*Whitney and Dilek,* 1998]. The Üçkapılı granite usually shows very weak ductile fabrics. It is locally associated with a dense array of dikes with variable orientations, cross-cutting at a high angle the foliation of the metamorphic rocks. These features might suggest that the emplacement of the Üçkapılı granite was post-tectonic. The

main body, however, has been identified as a late-kinematic intrusion, recording the same shearing deformation as its host rocks [*Gautier et al.,* 2002].

2.2. Previous Geochronology

Geochronological data on the Niğde Massif were first provided by *Göncüoğlu* [1986]. K-Ar dating of one muscovite and four biotite populations from samples of Üçkapılı-type granite and host Gümüşler gneisses in the northwestern part of the massif yielded ages of 78.5 ± 1.2 and 77.4 to 74.9 ± 1.2 Ma, respectively (Figure 3a). Rb-Sr data on the same five mineral separates were used by *Göncüoğlu* [1986] to define a mean mineral-whole rock isochron at 77.8 ± 1.2 Ma. Taken alone, the muscovite-whole rock pair yields an age of 78.7 Ma (recalculated from the analytical data). These mica ages have been used to infer cooling of both the granite and the host gneisses down to 300°C at ca. 78-75 Ma [*Göncüoğlu,* 1986; *Gautier et al.,* 2002].

Subsequently, Whitney and Dilek [1997, 1998] interpreted an unpublished U-Pb age on monazite at ca. 14-20 Ma from a sample of the Üçkapılı granite, at the center of the massif, as reflecting the age of crystallisation of the intrusion. Eleven fission track ages on apatite were obtained by *Fayon et al.* [2001] from samples of paragneiss and granite along a NW-SE transect across the Niğde Massif, clustering around 11-12 Ma. Based on these constraints, *Whitney and Dilek* [1997, 1998], *Fayon et al.* [2001] and *Whitney et al.* [2001] concluded that, following burial during Alpine crustal thickening, the metamorphic rocks of the Niğde Massif were exhumed as late as during the Early Miocene, finally reaching the surface during the Late Miocene. However, based on the field relations between the Niğde Massif and Paleogene sediments along its southern margin (see next section), *Gautier et al.* [2002] showed that both the Niğde high-grade metamorphic rocks and the Üçkapılı granite must have reached the surface before the Eocene, or at the beginning of Eocene times (before ca. 54 Ma) at the latest. The apatite fission track ages around 11-12 Ma necessarily reflect a later event, probably linked with widespread late Neogene magmatism in the region [*Gautier et al.,* 2002].

Since then, new $^{40}Ar/^{39}Ar$ and U-Pb (SHRIMP) geochronological data have been reported [*Whitney et al.,* 2003], lending support to the latter view. These data closely agree with, and extend, the earlier K-Ar and Rb-Sr dataset of *Göncüoğlu* [1986]. They can be summarized as follows. Southeast of Gümüşler, a garnet-biotite-sillimanite gneiss showing millimeter-scale migmatitic layering (sample 95-22 on Figure 2) yielded a U-Pb age on monazite at 84.7 ± 0.7 Ma (2σ; mean of 20 analyses on 14 grains). Zircons from a similar sample on the same outcrop appear mostly inherited from the sedimentary protolith; rare

overgrown rims gave a U-Pb age of 91.0 ± 2.0 Ma (2σ; mean of 3 analyses), interpreted by *Whitney et al.* [2003] as dating peak metamorphism and anatexis. However, judging from the narrowness of the rims, it seems difficult to rule out the possibility that the measured age was partly influenced by adjacent old mantles, so that the monazite U-Pb age may be viewed as a better constraint for the timing of peak temperature conditions. Further southeast, still in the Gümüşler migmatitic gneisses, hornblende from two amphibolites (samples 95-34 and 01-32) yielded $^{40}Ar/^{39}Ar$ plateau ages of 80.7 ± 1.1 and 78.8 ± 0.4 Ma (2σ). Close to Üçkapılı, a sample from the main body of Üçkapılı granite yielded zircons with usually an inherited core; seventeen analyses in the oscillatory-zoned mantles and rims gave U-Pb ages scattered between 91.5 and 76.8 Ma. Most of the higher-precision determinations cluster between 91.5 and ca. 85 Ma, with an uncertainty commonly less than 1.6 Ma (2σ). This age range is interpreted by *Whitney et al.* [2003] as the time of crystallization of zircons within distinct granitic magmas having subsequently coalesced. The younger age range, from ca. 85 to ca. 77 Ma, is interpreted as reflecting Pb loss at still high-temperature conditions, before the ascent and emplacement of the body. Finally, on the southeastern margin of the main Üçkapılı intrusion, biotite from a sillimanite schist (sample 95-59) yielded a $^{40}Ar/^{39}Ar$ plateau age of 76.2 ± 0.5 Ma (2σ).

2.3. Sediments Surrounding the Niğde Massif

The Niğde Massif is surrounded by sediments and volcanic rocks of variable age. To the north, Late Miocene-Pliocene ignimbrites and younger sediments nonconformably overlie the metamorphic series. To the south and southeast, most sediments are older, with the oldest deposits forming part of the Maastrichtian-Eocene Ulukışla Basin [e.g., *Görür et al.,* 1984; *Clark and Robertson,* 2002] (Figures 1 and 2). The contact relationship between these sediments and the underlying metamorphic rocks has formed the basis of contrasting interpretations in the literature. For most authors [e.g., *Göncüoğlu et al.,* 1991; *Yetiş et al.,* 1995], the overall sedimentary sequence lies nonconformably onto the high-grade rocks. In the lower part of the sequence, which mostly consists of deep marine turbidites interlayered with, then overlain by, basic to intermediate volcanic flows and volcanoclastic interbeds, fossils typical of the late Maastrichtian and of the Early and Late Paleocene were reported [*Göncüoğlu,* 1986; *Göncüoğlu et al.,* 1991]. The same age range, possibly extending into the Early Eocene, has recently been assigned to similar deposits further south in the Ulukışla Basin [*Clark and Robertson,* 2002]. Along the southern margin of the Niğde Massif, younger sediments consist of clastic deposits and shallow marine limestones of Eocene age

[*Göncüoğlu et al.,* 1991; *Yetiş et al.,* 1995]. Based on the benthic foraminifera species reported from these layers, *Gautier et al.* [2002] concluded that sedimentation spanned a period from the earliest Eocene to the early Middle Eocene (from ca. 54 to ca. 46 Ma). Recently, species from the mid-Middle Eocene have also been reported from this formation [*Dinçer and Avşar,* 2004]. Taken together, these constraints suggest continous shallow marine sedimentation from the earliest Eocene to the mid-Middle Eocene (from ca. 54 to ca. 42 Ma). Younger sediments consist of Oligocene to Neogene continental deposits [*Göncüoğlu et al.,* 1991; *Yetiş et al.,* 1995].

In contrast with earlier interpretations, and on the basis of their own radiometric data (see previous section), *Whitney and Dilek* [1997] and *Fayon et al.* [2001] claimed that those sediments older than the Middle or Upper Miocene do not nonconformably overlie the Niğde Massif, but are separated from it by a shallow-dipping extensional detachment fault along which the footwall rocks were exhumed as late as during the Early Miocene. However, *Gautier et al.* [2002] have shown that, at several locations around Çamardı, the sequence of Eocene shallow marine sediments overlies the high-grade metamorphic rocks of the Niğde Massif, as well as Üçkapılı-type granitic stocks, through a clear nonconformity, and reworks them as pebbles. On one hand, then, the metamorphic and granitic rocks must have been unroofed before about 54 Ma. On the other hand, the nonconformity of older sediments (late Maastrichtian to Late Paleocene) onto the Niğde Massif [*Göncüoğlu et al.,* 1991; *Yetiş et al.,* 1995] could not be confirmed [*Gautier et al.,* 2002]. The contact between the two, where not hidden by Eocene and younger nonconformable deposits, is a low-dipping fault zone. In the area of Kılavuz, the fault zone coincides with the detachment of *Whitney and Dilek* [1997] (Figure 2). Field relations suggest that at least part of the down-dip displacement along this fault is Neogene, unrelated to pre-Eocene exhumation of the Niğde Massif [*Gautier et al.,* 2002].

Importantly, clasts derived from the Niğde Massif seem absent from the late Maastrichtian to Late Paleocene sedimentary record near the massif, and more generally within the Ulukışla Basin [*Clark and Robertson,* 2002]. This strongly suggests that the high-grade rocks did not reach the surface before Late Paleocene times. This, in turn, suggests that, from the beginning, the Maastrichtian-Paleocene sediments and the high-grade rocks were juxtaposed due to faulting [*Gautier et al.,* 2002]. Faulting could have been active during or/and shortly after sedimentation, but before the onlap of nonconformable sediments from about 54 Ma onward. Additional evidence for a change in tectonic environment around the Paleocene-Eocene boundary includes (1) a pronounced angular unconformity at the interface

between Maastrichtian-Paleocene and Eocene series near Çamardı [*Yetiş et al.,* 1995], (2) the contemporaneous drastic change from deep marine to shallow marine conditions of sedimentation in the vicinity of the Niğde Massif, and more generally in the whole Ulukışla Basin, where this change also coincides with an abrupt lowering in subsidence rate [*Clark and Robertson,* 2002].

3. Structural Analysis

3.1. A Metamorphic Dome

As pointed out in section 2.1, two main structural units are distinguished in the Niğde Massif [see also *Gautier et al.,* 2002]. Much of the massif exposes rocks from the lower unit (Figure 2). All the metamorphic rocks in the lower unit are pervasively foliated. Primary compositional layering in the metasediments and in the metabasic rocks has been transposed into parallelism with the penetrative foliation, attesting for high strain intensities. Recumbent tight to isoclinal folds are common, confirming this view. Foliation planes have low to moderate dips. Foliations commonly dip away from the center of the Niğde Massif, a feature that is best expressed along its margins (Figure 4). A fairly concentric pattern of foliation planes can be recognized in the western part of the massif, lying subparallel to the boundaries between the main lithological formations (Figure 5). Consequently, foliations in the lower unit define a broad dome, and most of the Niğde Massif can be described as a metamorphic dome. The core of the dome, in the northwestern part of the massif, exposes the deeper levels of the lower unit, made up of Gümüşler paragneisses showing pervasive migmatization (Figure 3a). Distinct structures are observed at various levels of the lower unit, as described below.

3.2. Deeper Levels of the Lower Unit

The deepest levels of the lower unit, exposed in the core of the dome, are characterized by the development of a pronounced stretching lineation with a consistent trend at about N20° (Figure 5). Shear sense criteria consistently document top-to-SSW shearing (Figure 7). In the area immediately southeast of Gümüşler, the location of sample 95-22 of *Whitney et al.* [2003] (see section 2.2), metatexitic migmatites display 1 to 10 cm-thick low angle shear bands along which the products of melting have been collected (Figures 7a and 7b). This indicates that top-to-SSW shearing and migmatization were contemporaneous. More often, however, leucosomes are tightly folded and transposed into parallelism with the external foliation (Figure 7c), which itself is consistently bent into sigmoids by a set of low angle shear bands (Figure 7d). This shows that top-to-SSW shearing continued after migmatization ended.

Most Üçkapılı-type intrusions in the core area show no ductile fabric, a number of them occurring as thick dikes cross-cutting at a high angle the shallow-dipping foliation. This suggests that, at the time these intrusions emplaced, the host rocks had cooled enough to behave brittlely and(/or) top-to-SSW shearing deformation had already vanished. Meanwhile, the crustal origin of Üçkapılı-type magmas indicates that extensive migmatization was still under way deeper in the metamorphic pile. The youngest structures observed in the core area consist of decimeter- to meter-thick semi-brittle shear zones (Figures 5 and 8b) and brittle normal faults consistently dipping, at low to moderate angles, to the north-east or north-northeast (Figures 2, 3b, and 8a). This observation suggests that top-to-SSW shearing indeed vanished in the deepest exposed part of the lower unit, being replaced by top-to-NE/NNE brittle shearing, when temperature conditions became too low to sustain ductile deformation. More precisely, we have no firm constraint on the age of faulting; among the faults within the dome, some may be recent or recently reactivated faults, like the large NNW-SSE steep fault zone crossing the whole massif (Figures 2 and 3b) [see also *Toprak and Göncüoğlu,* 1993]. Nevertheless, we believe that the faults seen in the core area were formed during pre-Eocene exhumation, soon after top-SSW ductile shearing, on account of (1) their semi-brittle character (Figure 8b), (2) despite a slight obliquity, their kinematic compatibility with ductile to brittle shearing at higher levels of the lower unit (Figures 3b and 5), (3) their strikingly low dips (Figures 3b, 8a, and 8b) in comparison with the steepness of most post-Eocene faults in the region [e.g., *Toprak and Göncüoğlu,* 1993; *Jaffey and Robertson,* 2001].

Although rare, syn-kinematic granitic intrusions are also present in the core area, in the form of meter-thick dikes slightly oblique or parallel to the foliation of the host rocks. Such a dike can be observed in the valley south of Gümüşler (Figure 8c). The granite is fine-grained and shows the homogeneous development of a C-S fabric [*Berthé et al.,* 1979] consistent with top-to-SSW shearing (Figure 8d). The C-S fabric is somehow non typical, in the sense that C planes are not highly localized shear surfaces but consist of penetrative shear bands. Along them, biotite flakes lie parallel to the fabric and lack kink bands, while quartz aggregates retain the same interlobate texture, with no grain shape preferred orientation, as outside the shear bands. Flattened feldspar grains remain untwinned and lack fractures. On one hand, these features indicate that deformation occurred at temperatures above about 450°C (i.e., above greenschist facies conditions) [e.g., *Simpson,* 1985]. On the other hand, the pervasive development of a C-S fabric indicates that at least part of the deformation occurred at temperatures below about 550°C [cf. *Gapais,* 1989]. The presence of macroscopic shear bands within the migmatitic paragneisses (Figure 7d) supports this view. Thus, top-to-SSW

shearing at deeper levels of the lower unit was still active at temperature conditions around 500°C, but may have vanished as early as during cooling below 450°C.

In summary, the core of the dome shows evidence for syn- to post-migmatization ductile top-to-SSW shearing followed by top-to-NE/NNE semi-brittle to brittle shearing. This sequence of events seems opposite to the one suggested by *Whitney et al.* [2003] for the same area (pervasive top-to-NNE shearing, then top-to-SSW shearing along localized shear bands). Nevertheless, our observations document the pervasive, high- to medium-temperature character of the top-to-SSW shearing deformation (Figures 7 and 8d), and the localized, low-temperature character of top-to-NE/NNE shearing (Figures 8a and 8b).

3.3. Higher Levels of the Lower Unit

Higher levels of the lower unit are also characterized by the development of a pronounced stretching lineation, although with a more scattered pattern of orientations than observed at deeper levels (Figure 5). Nevertheless, a mean trend around N60° is recognized over much of the area, except at the eastern margin of the massif, where a few measurements document NNW-SSE-trending lineations. With one exception at the margin of a large apophysis of the Üçkapılı granite, all sites where shear sense indicators could be found document top-to-NE shearing. The transition from deeper levels, showing top-to-SSW shearing, to higher levels, showing top-to-NE shearing, is sharp. On three sites where the lowermost part of higher levels could be seen (marked with a star on Figure 5), part of the outcrop shows a steep foliation underlined by migmatitic layering being tightly folded and crenulated in between low-dipping top-to-NE shear bands (Figure 9a).

Üçkapılı-type intrusions emplaced at higher levels of the lower unit are variably deformed. Most dikes show a very weak or no ductile fabric. The main body of granite has already been described as a late-kinematic intrusion, displaying top-to-NE C-S fabrics only locally, at its roof, while a weak ductile fabric, with a NE-dipping foliation and a NE-SW-trending lineation, characterizes the interior of the pluton [*Gautier et al.,* 2002] (Figures 4 and 5). In the same area where the C-S fabrics are observed, ultracataclastic joints up to 5 cm in thickness occur locally, dipping at a low angle toward the northeast (Figure 9b). Where the joints occur, the C-S fabric dips toward the southwest, which is consistent with the fabric having been back-tilted between top-to-NE brittle shear bands. Finally, a few intrusions show a pervasive development of C-S fabrics. Such an intrusion, undescribed until now, is exposed for about 1 km along a river bed in the northern part of the massif (Figures 3b and 5). The C-S fabric in it documents top-to-ENE shearing (Figures 10a and 10b). Only the topmost 30 m of

the pluton are exposed, therefore it is not known whether deeper levels of the intrusion would also display the pervasive C-S fabric. Another such intrusion is a NW-SE-trending dike of fine-grained granite, about 100 m in thickness, intruding the Aşıgediği formation on the southern limb of the dome. Here again, the pervasive C-S fabric indicates top-to-NE shearing (Figure 5).

3.4. Contact Zone with the Upper Unit

Approaching the contact with the upper unit, strain intensity significantly increases in rocks of the lower unit. Strong deformation and transposition being the rule in the metamorphic rocks throughout the lower unit, the increase is better documented when focusing on syn-kinematic intrusions. In the north-central part of the massif, on a roadcut exposure about 50 m below the contact itself (Figures 3b and 5), granite intrusions are converted into fine-grained ribbon mylonites concordant with the foliation of the host paragneisses (Figures 11a and 11b). Most paragneisses show a relictic migmatitic texture in the form of 0.5 to 3 cm-thick stretched and boudinaged quartz + feldspar ± muscovite segregations (Figures 11c and 11d), interpreted as leucosomes, embedded into <5 mm-thick biotite ± sillimanite layers, interpreted as melanosomes. Pronounced stretching lineations trend in a mean direction of N78°. Shear sense criteria such as asymmetric boudinage of quartz-feldspar segregations (Figure 11c) and, in thin sections within mylonitized intrusions, mica fishes and σ-type feldspar porphyroclasts (Figures 11e and 11f), indicate penetrative top-to-ENE shearing. In the same exposure, low angle localized shear bands (Figure 11d), meter-thick semi-brittle shear zones with striations trending parallel to the earlier stretching lineation, and NE-dipping normal faults (Figures 11a and 11b) give the same kinematics, documenting a decrease in temperature during shearing. The contact itself, although poorly exposed, shows semi-brittle shear zones and a ~3 m-thick array of ultracataclastic faults.

Ultracataclasites and thick microbreccias are also found along the southern margin of the dome (Figure 5). Close to Çamardı, a layer of dark green massive ultracataclasites several meters thick directly underlies the nonconformable Eocene sediments [see *Gautier et al.,* 2002, their Figure 6b]. The sediments themselves being pervasively schistosed, cataclasis potentially resulted from post-Eocene deformation. In neighboring sections, however, pervasively schistosed Eocene sediments overlie the metamorphic basement without an intervening layer of cataclasites. Therefore, ultracataclasis near Çamardı likely predates the Eocene sedimentation [*Gautier et al.,* 2002]. Support for this interpretation is found further west, close to Celaller, where decimeter-thick ultracataclastic joints within paragneisses and

quartzites of the lower unit are truncated nonconformably by a series of conglomerates and microconglomerates similar to those at the base of the Eocene sequence (Figures 12a and 12b). In contrast with the situation near Çamardı, both the rugged erosional surface defining the nonconformity and the overlying sediments are tilted but not strained. The ultracataclastic joints cross-cut at a right angle both the foliation and the stretching lineation of the metamorphic rocks (Figure 12a), indicating ongoing NE-SW stretching during cooling. These features suggest that the area of Çamardı and Celaller provides another example of the contact zone with the upper unit, characterized by strong cataclasis, although the upper unit itself is not exposed (Figure 3a).

Further west, the area of Kılavuz shows the development of reddish-purple microbreccias associated with ferric oxi-hydroxide mineralizations (Figure 5). Abundant fine-grained granitic dikes occur in the same area. They often exhibit a greenish color due to pervasive hydrothermal alteration, while brecciation and ferric oxi-hydroxide mineralization sometimes develop along them. The dikes are steep and trend consistently NW-SE; some of them contain abundant cm-thick quartz veins of similar orientation (Figure 12e). On one hand, this documents ongoing NE-SW stretching while the rocks cooled down to the conditions of brittle deformation. On the other hand, intense microbrecciation has preferentially developed along several shear zones up to 4 meters-thick, dipping at low to moderate angles toward the south-southeast. Fluid-assisted deformation along these shear zones has produced graded microbreccias (Figure 12c) with occasionally subrounded to well rounded clasts (Figure 12d), giving the rocks the appearance of reddish microconglomerates and sandstones [see *Anders et al.,* 2000, for other examples and a discussion]. The shear zones are located within quartzites or along the interface between quartzites and marbles. In the latter case, decimeter to meter-thick tension gashes run from the shear zone into the marbles, filled with quartzite clasts mixed with a few marble blocks. Therefore, at least part of this deformation occurred at temperatures below about 300°C. One of these finely laminated shear zones displays stretching lineations with a consistent N-S trend. Thus, brittle deformation along the southwestern margin of the dome apparently included a component of N-S shearing, developed either contemporaneously or after NE-SW stretching.

4. $^{40}Ar/^{39}Ar$ Dating

4.1. Analytical Method

$^{40}Ar/^{39}Ar$ data were obtained at the "Laboratoire Magmas-Volcans" in Clermont-Ferrand, France, using a mass spectrometer VG3600. The samples were irradiated at the University of Michigan Ford Nuclear Reactor in position L67 during 28 hours. J factor was estimated by the use of the Fish Canyon sanidine standard, with an age of 28.48 ± 0.06 Ma [*Schmitz and Bowring,* 2001], at a value of 0.00431 with 1% relative standard deviation. $^{40}Ar/^{39}Ar$ analyses were performed on amphibole, muscovite and biotite bulk samples (around 5-10 mg) loaded in aluminium packet into a double vacuum furnace and analyzed by the step-heating procedure described in *Arnaud et al.* [1993]. Age calculations are given at 2σ and include all correction factors as well as errors on blanks. Detailed analytical results are available from the authors upon request.

4.2. Results

Amphibole grains were separated from sample N8, a finely foliated amphibolite from the southern flank of the dome (Figure 2). On the outcrop and in thin section (Figure 13a), amphiboles are aligned parallel to the NE-SW-trending stretching lineation seen in this part of the dome. The age spectrum yields a plateau age of 81.65 ± 1.10 Ma (92.9 % of the ^{39}Ar released) (Figure 13b). The spectrum is strongly controlled by two steps, at 1100 and 1200°C, during which most of the ^{39}Ar was released. The $^{39}Ar_K/^{37}Ar_{Ca}$ ratio, which is proportional to K/Ca, decreases with increasing temperature and converges toward a constant value for the fraction corresponding to the plateau age (Figure 13b). This means that the fraction of argon released during the three steps defining the plateau age originates from a chemically homogeneous part of the amphibole grains.

Biotite grains were separated from sample N13, a syn-kinematic granitic dike described in section 3.2 (Figures 8c and 8d), and from sample N49, within the main body of Üçkapılı granite (Figure 2). Both samples are characterized by an increasing age spectrum that does not define a strict plateau age (that is, three successive steps covering at least 70% of the ^{39}Ar released). This could be due to chloritization, although this has not been observed in thin sections. The N13 spectrum (Figure 8e) yields minimum and maximum ages of 34 and 78 Ma, respectively, and concordant apparent ages at 75.01 ± 0.84 Ma at high temperature (four steps representing 55.9 % of the ^{39}Ar released). The N49 spectrum (Figure 13c) yields minimum and maximum ages of 28 and 120 Ma, respectively, and concordant apparent ages at 75.09 ± 1.03 Ma at high temperature (three steps representing 64.3 % of the ^{39}Ar released, i.e., a pseudo-plateau age).

Muscovite grains were separated from samples N16, N44 and N67 (Figure 2). N16 comes from a syn-kinematic two-mica granite described in section 3.3 (Figures 3b, 5, and 10). In thin section, muscovite is aligned parallel to the C-S fabric (Figure 10b). N44 is a mylonite from the roadcut exposure described in section 3.4 (Figures 3b, 5, and 11). In thin section, muscovite consists of finely recristallized grains aligned parallel to the mylonitic fabric, and coarser fish-type clasts (Figure 11f). N67 comes from a two-mica granitic intrusion in the southeastern flank of the dome, showing a slight but pervasive, dominantly linear fabric oriented 32°SW/N52°, i.e., subparallel to the ENE-WSW stretching lineation in the host rocks (Figure 5). In thin section, muscovite consists of large grains texturally in equilibrium with the other magmatic phases. The N16 spectrum (Figure 10c) yields a plateau age of 78.05 ± 0.84 Ma (85.3 % of the ^{39}Ar released). N44 shows a saddle-shaped spectrum (Figure 11g) with concordant apparent age minima at 75.92 ± 0.88 Ma (three steps representing 51.3 % of the ^{39}Ar released). The N67 spectrum (Figure 13d) yields a plateau age of 76.01 ± 0.78 Ma (94.2 % of the ^{39}Ar released).

The data described above, together with radiometric and biostratigraphic constraints from the literature (see sections 2.2 and 2.3), are summarized in Figure 3 and synthesized in a temperature-time diagram (Figure 14). Closure temperatures used in Figure 14 are typical ones, except for argon in muscovite. In this case, we adopted a conservative value of 400 ± 75°C, taking into account studies [e.g., *Kirschner et al.,* 1996] suggesting significantly higher temperatures than the usual value of 350±50°C.

5. Interpretation of Deformation at Higher Levels of the Dome

5.1. Ductile to Brittle Shearing along an Extensional Detachment

The structural evolution recorded by rocks at higher levels of the lower unit and along the contact zone with the upper unit is typical for extensional detachment zones [e.g., *Lister and Davis,* 1989]. Top-to-NE/ENE shearing is recorded from the conditions of pervasive ductile deformation to those of localized brittle faulting, showing that deformation developed during cooling and exhumation. Shearing has localized toward the roof of the lower unit, resulting in a ~100 m-thick fault rock sequence with a vertical superposition of brittle upon ductile large strain fabrics (Figure 11), a feature typically encountered along extensional detachments once rooted in the middle or lower crust [e.g., *Lister and Davis,* 1989; *Gautier et al.,* 1993]. Ultracataclasites are found at the top of the lower unit, above which the ophiolitic rocks of the upper unit show very limited post-magmatic deformation (Figure 6). Thus, the

contact between the lower and upper units bears all the structural elements of a ductile to brittle extensional detachment (Figure 3b). As pointed out in section 2.1, the upper unit has experienced significantly lower peak conditions of metamorphism than the lower unit has, a feature also expected for a normal-sense shear zone with a large offset.

Because highly localized greenschist facies deformation is restricted to the base of the upper unit (Figure 6b), it may be thought to result also from shearing along the extensional detachment. Alternatively, it may date from the emplacement of the ophiolitic nappe, the basal thrust zone being subsequently cut or reactivated by the extensional shear zone at shallower depth conditions. The strong cataclasis seen along the contact between the two units is more in line with the latter interpretation. Although kinematic data may have helped to solve the question, none were obtained from the greenschist facies shear zones.

5.2. Associated Development of a Cordilleran-Type Core Complex

5.2.1. Kinematics of Extension and Asymmetry of the Core Complex

Given that an extensional detachment overlies the high-grade metamorphic dome (Figure 3a), the Niğde Massif as a whole can be described as a typical Cordilleran-type metamorphic core complex, in agreement with *Whitney and Dilek* [1997]. At variance with these authors, however, the main extensional shear zone does not lie along the southern margin of the dome but in the northern part of the massif, the massive gabbros forming the hangingwall of the detachment (Figures 2 and 3). According to the early work of *Whitney and Dilek* [1997], the kinematics of ductile extensional shearing was top-to-NE in the northern part of the dome and top-to-SW in the southern part, so that the core complex could be described as doubly vergent. More recently, *Whitney et al.* [2003] have argued that top-to-NE/NNE shearing represents an earlier fabric of unknown origin, while top-to-SW/SSW shearing represents the dominant kinematics of extension. In contrast, our analysis reveals top-to-ENE(/NE) ductile to brittle shearing along the main detachment zone (Figures 3b and 11). We consider therefore that the core complex has developed in response to shearing along a major NE/ENE-dipping detachment (Figures 15a and 15b). As discussed in section 3.2, top-to-SSW shearing in the core of the dome is overprinted by, and, therefore, is older than, top-to-NE shearing. On the scale of the Niğde massif, the restriction of higher levels of the lower unit (Aşıgediği formation) to the southwest (Figure 2) is in line with the expected asymmetry of the core complex if indeed controlled by a major NE/ENE-dipping detachment. In the souhwestern flank of the dome, i.e., in the part of the dome opposite to the initial direction of dip of the detachment, the mean dip of foliation planes is around 40° (Figure 4). Following the

argument of *Brun and Van den Driessche* [1994] [see also *Gautier et al.*, 1993], this suggests that the initial dip of the detachment zone was also 40°, to the northeast (Figures 15a and 15b).

In Figure 15a, we assume that, from the beginning of extension, a continuous detachment zone existed from the surface down to the lower crust, as in classical interpretations [e.g., *Lister and Davis,* 1989]. Based on numerical modeling, *Tirel et al.* [2004] recently pointed out that early stages of core complex-type extension may not involve such a continuous detachment zone. Instead, early extension may be more symmetrical [see also *Brun et al.,* 1994; *Tirel et al.,* 2006] and involve two separate zones of high strain that ultimately connect at middle crustal depths to build a typical detachment. Based on a comparison between active faulting in the Gulf of Corinth and earlier detachment-type extension in the Cyclades Islands, *Jolivet et al.* [2004] and *Mehl et al.* [2005] also suggested that the brittle segment of low-dipping detachments may form only lately during extension, resulting from the upward propagation of ductile shear zones originated near the brittle-ductile transition zone. As we see no obvious way to test these hypotheses in the case of the Niğde dome, we leave it open whether they represent a viable alternative. Irrespective, extension became asymmetrical, controlled by a major NE/ENE-dipping detachment (Figure 15b).

5.2.2. A Wrench-Controlled Core Complex?

Modifying *Whitney and Dilek* [1997]'s initial interpretation, *Whitney et al.* [2001] and *Fayon et al.* [2001] later proposed that the Niğde massif represents a core complex developed within a broad zone of wrenching paralleling the Central Anatolian Fault Zone, a NE-SW-trending fault zone that bounds the CACC on its eastern side [*Koçyiğit and Beyhan,* 1998]. In the study area, the Central Anatolian Fault Zone is represented by the Ecemiş Fault Zone, running NNE-SSW along the eastern margin of the Niğde Massif (Figure 2). The Ecemiş Fault Zone, which records about 60 km of sinistral offset [e.g., *Jaffey and Robertson,* 2001], is interpreted by *Whitney et al.* [2001] and *Fayon et al.* [2001] as resulting from late localized shearing along the eastern wall of the wrench zone. However, there is convincing evidence that most, if not all, of the sinistral displacement along the fault accumulated after the Late Eocene [*Jaffey and Robertson,* 2001], i.e., at least 20 Ma after extensional unroofing of the Niğde high-grade rocks. Thus, as discussed by *Gautier et al.* [2002], core complex-type extension in the Niğde Massif and sinistral shearing along the Central Anatolian Fault Zone are better viewed as two separate events. Another argument comes from the attitude of foliations along the eastern margin of the Niğde Massif, which dip at about 35° to the

southeast (Figure 4). In the same area, nonconformable Oligocene sediments have a similar dip (Figure 4), the mean being only around 3° lower than that of the underlying metamorphic rocks. Rotating back the tilt of the sediments, this shows that, at a distance of only 5 km from the eastern wall of the inferred wrench zone, foliations were actually subhorizontal (like in Figure 6 of *Fayon et al.* [2001]), a picture contrasting with what is known from well-documented wrench-controlled core complexes [*Leloup et al.,* 1995; *Jolivet et al.,* 2001]. We conclude that there is no clear evidence for wrenching during the pre-Eocene development of the Niğde core complex.

In contrast, the high-intensity low-grade deformation affecting Eocene nonconformable sediments and earlier deposits along the southeastern margin of the massif [*Gautier et al.,* 2002] (see also section 3.4) might be interpreted as resulting from strike-slip displacement along the Ecemiş Fault Zone. An apparent support to this hypothesis is that this deformation is recorded to the northeast of Celaller only, i.e., along the margin of the massif that is the closest to the fault zone. However, shear sense criteria associated with this low-grade deformation consistently indicate top-to-W/SW shearing along schistosity planes moderately dipping toward the east or southeast (Figures 4 and 5). This documents a component of dextral shearing at a low angle to the trace of the Ecemiş Fault Zone but with opposite kinematics. This, in turn, strongly suggests that the low-grade deformation predates high-magnitude sinistral shearing along the Ecemiş Fault Zone. The Oligocene sediments at the eastern margin of the massif do not display the low-grade deformation and are reported to cover unconformably the Early-Middle Eocene sequence [*Göncüoğlu et al.,* 1991; *Yetiş et al.,* 1995]. These relations indicate that the low-grade deformation is older than the latest Oligocene (but younger than the mid-Middle Eocene, cf. section 2.3). They also suggest that the maximum possible age of sinistral shearing along the Ecemiş Fault Zone is earliest Oligocene, in agreement with the arguments of *Jaffey and Robertson* [2001].

6. Timing of the Two Main Shearing Events

The timing of deformation in the Niğde Massif is discussed in the light of available constraints, summarized in Figure 14. A temperature-time path can be drawn using radiometric data from deeper levels of the lower unit. The path yields a mean cooling rate of about 60°C/Ma during cooling from ~700 to ~300°C, similar to rates obtained in other extensional core complexes [e.g., *Dallmeyer et al.,* 1986; *Gautier et al.,* 1993; *Vanderhaeghe et al.,* 2003].

The timing of the two main shearing events identified in the lower unit (top-to-NE/ENE at higher levels vs. top-to-SSW at deeper levels) is determined using constraints labelled 'a' to 'd'. Constraint 'a' (at 84.0 Ma), which is the younger limit of the U-Pb age on monazite from sample 95-22 of *Whitney et al.* [2003], is taken as the latest possible date for the onset of top-to-SSW shearing. This arises from the fact that this age was obtained in a migmatitic paragneiss from the same locality (Figure 2) where we observed the most striking evidence for top-to-SSW shearing during migmatization (Figures 5, 7a, and 7b). Constraint 'b' (at 80.55 Ma), which is the younger limit of the $^{40}Ar/^{39}Ar$ age on hornblende from sample N8 (Figure 13b), is taken as the latest possible date for the onset of top-to-NE/ENE shearing. This arises from the fact that the amphiboles in this sample from near the southern margin of the massif (Figure 2) are aligned parallel to the NE-SW-trending stretching lineation seen in this part of the dome, with consistent top-to-NE shear sense criteria in neighboring exposures (Figure 5). Constraint 'c' (at 79.0 Ma) is the earliest possible date for the end of top-to-SSW shearing. As discussed in section 3.2, structural evidence indicates that top-to-SSW shearing in the core of the dome was still active at temperature conditions around 500°C and had vanished when the rocks were cooled down to the conditions of brittle deformation, possibly as early as during cooling below 450°C. Constraint 'c' is then defined as the intersection between the 500°C temperature axis and the temperature-time path of the rocks. The path itself runs along the older limit of the $^{40}Ar/^{39}Ar$ age on biotite from sample N13, a granitic dike having experienced top-to-SSW shearing at temperatures above 450°C (Figures 8d and 8e). Constraint 'c*' (at 82.3 Ma) is taken as an alternative end member case, where the 500°C temperature axis intersects the left margin of the temperature-time "wider band" defined in Figure 14. Finally, constraint 'd' (at 76.8 Ma), which is the older limit of the $^{40}Ar/^{39}Ar$ age on muscovite for both samples N44 (Figure 11g) and N67 (Figure 13d), is taken as the earliest possible date for the end of top-to-NE/ENE shearing. Sample N44 is a mylonite from the detachment zone, at higher levels of the lower unit (Figure 3b), with muscovite grains aligned in the mylonitic fabric (Figure 11f). Because top-to-ENE shearing has persisted in the detachment zone while the rocks cooled down to the conditions of brittle deformation, top-to-NE/ENE shearing was probably still active after 76.8 Ma. Sample N67 comes from a granite stock in the southeastern flank of the dome (Figure 2), showing a slight but pervasive linear fabric subparallel to the ENE-WSW stretching lineation in the host rocks (Figure 5). The intrusion is much less than 1 km thick, therefore it cooled fast enough for the muscovite age to be taken as a reasonable approximation of the time at which this late-kinematic intrusion recorded the regional deformation.

In summary, a minimum time range can be determined for the two shearing events (Figure 14). Top-to-NE/ENE shearing at higher levels of the lower unit lasted at least 3.75 Ma. Top-to-SSW shearing at deeper levels lasted at least 5.0 Ma, using constraint 'c', or 1.7 Ma, using constraint 'c*'. In the former case, a time overlap of at least 1.55 Ma is found, showing that the two shearing events were contemporaneous, at least in part. In the end-member latter case, there is no ascertained time overlap, nevertheless the time gap between the two shearing events is only 1.75 Ma, at most. Constraint 'b' arises from our $^{40}Ar/^{39}Ar$ amphibole age on sample N8, while constraints 'c' and 'c*' largely arise from two $^{40}Ar/^{39}Ar$ amphibole ages obtained by *Whitney et al.* [2003] (Figure 14). *Whitney et al.* [2003] used an age of 27.84 Ma for the Fish Canyon sanidine standard, whereas we used 28.48 ± 0.06 Ma [*Schmitz and Bowring,* 2001]. If, for consistency, we recalculate the age of N8 using the value of *Whitney et al.* [2003], the above largest possible time gap becomes 2.45 Ma. It seems unlikely that a major reorganization in regional tectonics could have occurred within such a brief time interval, and it would be highly coincidental to have it recorded in the short life of a rapidly cooling metamorphic dome. We thus consider that the evidence is strong enough to indicate that the two shearing events were broadly contemporaneous. Consequently, they must reflect some kind of strain partitioning at some depth in the crust during a single tectonic event. This tectonic event involved the development of an extensional core complex and lasted from ≥84.0 Ma to <76.8 Ma, i.e., at least 7.2 Ma, which is consistent with estimates of the characteristic lifetime of extensional core complexes [e.g., *Gautier et al.,* 1993; *Vanderhaeghe et al.,* 2003; *Tirel et al.,* 2004].

7. Significance of Oblique Ductile Shearing in the Core of the Dome

7.1. Summary of the Relations between the Two Main Shearing Events

The origin of top-to-SSW shearing in the core of the Niğde dome must be discussed in the light of its relation with top-to-NE/ENE shearing at higher levels of the lower unit, which itself has been shown to be linked to the development of an extensional detachment. Three main features characterize this relationship. First, the two shear directions are significantly oblique in the horizontal plane, making an angle of about 40° when considering a mean N60° trend of the stretching lineation at higher levels of the lower unit (Figure 5). The angle reaches 58° when considering a mean N78° trend of the stretching lineation in the ~100 m-thick zone of mylonites underneath the contact with the upper unit (i.e., the zone of localized strain defining the detachment). Second, the two shearing events were broadly contemporaneous.

More precisely, Figure 14 suggests that they were active together while the rocks of the lower unit experienced temperatures around 500°C, reflecting a process of strain partitioning in the lower-middle crust. Third, migmatites apparently played a role in the relationship between the two shearing events. Top-to-SSW shearing is restricted to the deeper, migmatitic part of the lower unit (Figures 2, 3, and 5), was active during migmatization (Figures 7a and 7b), and vanished when the rocks were cooled down to the conditions of brittle deformation, possibly as early as during cooling below 450°C. Later deformation in these migmatites involved limited top-to-NE/NNE semi-brittle to brittle shearing (Figures 8a and 8b). In contrast, the topmost migmatites experienced intense top-to-ENE shearing along the detachment zone, starting from the conditions of ductile deformation (Figures 3b and 11). In other words, the sharp spatial transition from top-to-SSW to top-to-NE/ENE ductile shearing is located within the dome of migmatites, near its top. These features suggest that strain partitioning was favored, and possibly triggered, by the presence of migmatites.

7.2. Extension of the Migmatite Dome at Depth

The thickness of the migmatitic body, beneath the apex of the Niğde dome, can be estimated as follows. As discussed in section 3.2, most Üçkapılı-type intrusions in the core area show no ductile fabric, a number of them occurring as steep dikes. Since Üçkapılı-type magmas derive from the continental crust, this indicates that extensive migmatization was still under way at some depth while the core rocks had cooled enough to escape top-to-SSW ductile shearing. Therefore, at this time, the core rocks were cooler than about 450°C. Migmatization at greater depth must have occurred at temperatures above 650°C, probably around 750°C. With a geothermal gradient in the range of 32 to 43°C/km (i.e., the range that can be deduced from the estimated peak P-T conditions in the core area, cf. section 2.1), the corresponding difference of >200-300°C is equivalent to a difference in depth in the range of >4.7 to 9.4 km. Likewise, a temperature difference between the core rocks and contemporaneous migmatization at depth can be derived from the $^{40}Ar/^{39}Ar$ age on muscovite from sample N67, at 76.0 ± 0.8 Ma (Figure 13d). Because this late-kinematic two-mica intrusion is small, it cooled rapidly, therefore the age closely approximates a period of anatexis at greater depth. At this time, according to the temperature-time path drawn in Figure 14, temperatures in the core area were probably in the range of 260 to 350°C, or up to 460°C according to the temperature-time “wider band”. Thus, the temperature was >190 to 490°C lower than that of migmatization, equivalent to a depth difference in the range of >4.4 to 15

km. We take these estimates as evidence that the body of migmatites seen in the core of the Niğde dome has a significant downward extent (at least 5 km).

In doing so, we assume that migmatization was an almost continuous process in space and time; that is, no significant gap exists between the migmatites in the core of the dome (at higher-temperature conditions at ca. 85 Ma), and those at greater depth, deduced from later Üçkapılı-type intrusions. As discussed above, one such intrusion has emplaced as late as ca. 76 Ma. Another one is the syn-kinematic two-mica granite that yielded a $^{40}Ar/^{39}Ar$ age on muscovite at 78.0 ± 0.8 Ma (Figure 10). Taking into account the relatively large size of the intrusion (Figure 2), this age suggests that the granite has emplaced at around 78-80 Ma, i.e., only about 5-7 Ma after the record of higher-temperature conditions in the core of the dome. *Whitney et al.* [2003] suggested that, during the period from ca. 85 to ca. 77 Ma, zircons from the main body of Üçkapılı granite were experiencing Pb loss at still high-temperature conditions, before the ascent and emplacement of the intrusion (see section 2.2). An emplacement later than ca. 77 Ma is consistent with our biotite $^{40}Ar/^{39}Ar$ age on sample N49 at 75.1 ± 1.0 Ma (Figure 13c). Taken together, these features are more in line with the assumption of subcontinuous migmatization from the core of the dome downward, for at least 5 km, rather than with an interpretation that would involve several zones of anatexis at significantly different depths.

Finally, it is worth emphasizing that, starting from ca. 82 Ma, not the whole of this >5 km-thick pile was anatectic, as the exposed migmatites were already cooler than 650°C (Figure 14). Therefore, on a timescale of about 9 Ma (from ca. 85 to ca. 76 Ma), migmatization has been maintained beneath the apex of the core complex while fast cooling due to extensional exhumation led progressively deeper parts of the migmatitic body to get out of the conditions of anatexis.

7.3. Favored Interpretation: Lateral Underflow during Cordilleran-Type Extension

7.3.1. Lateral Underflow

Our favored interpretation for the origin of oblique shearing in the core of the Niğde dome involves a process of lateral flow of the lower crust in response to highly localized extension in the middle and upper crust (Figures 15b and 15c) and/or high-magnitude extension on the regional scale (Figure 15d). Since the early 90s, horizontal flow of the lower crust, thought to be possible if the crust is of sufficiently low viscosity (e.g., due to anatexis), has often been proposed as an efficient means to keep the Moho flat during core complex-type extension [*Block and Royden,* 1990; *Wernicke,* 1990; *Buck,* 1991; *Wdowinski and Axen,* 1992;

Brun and Van den Driessche, 1994; *McKenzie et al.,* 2000; *Tirel et al.,* 2004; *Teyssier et al.,* 2005]. A feature common to all these models is that they are two-dimensional, so that "inward" or "channel" flow in the lower crust necessarily proceeds in a direction parallel to the direction of extension at shallower levels. However, in three dimensions, lateral (i.e., orthogonal or highly oblique) flow seems also feasible. In the following, this is called lateral "underflow", to emphasize its location beneath the part of the metamorphic pile undergoing extensional shearing along the detachment zone (Figures 15b and 15c). So far, underflow at right angles to the direction of extension has been described in only a few examples of gneiss domes [*MacCready et al.,* 1997; *Andronicos et al.,* 2003; *Amato and Miller,* 2004]. When applied to the Niğde dome, underflow seems to have proceeded not at right angles to the direction of extension but with a significant obliquity (about 58°). In one of the above examples [*Amato and Miller,* 2004], suborthogonal flow is recorded through a progressive rotation of the stretching lineation across a thickness of 7 km within the metamorphic pile. In the Ruby Mountains core complex, *MacCready et al.* [1997] also describe a transitional zone characterized by an intermediate trend of the stretching lineation. In the Niğde dome, this transitional zone could coincide with the part of the lower unit displaying top-to-NE shearing, in between the mylonitic detachment zone (top-to-ENE) and the deepest exposed levels (top-to-SSW) (Figure 5). Considering that the exposed pile of rocks showing top-to-SSW shearing is only about 1 km thick (Figure 3a), it is possible that the lineation rotates even further with depth below the present surface, so that strictly orthogonal underflow may also apply in the case of the Niğde dome.

7.3.2. Strain Partitioning and Structural Domains within the Migmatite Dome

Horizontal flow is generally thought to require a lower crust of very low viscosity [e.g., *Block and Royden,* 1990; *Buck,* 1991; *Kruse et al.,* 1991; *McKenzie et al.,* 2000], which is consistent with the record of lateral underflow within the migmatitic part of the Niğde dome. However, this observation does not imply that the lower crust was homogeneously anatectic on a regional scale. Instead, migmatization could have been restricted to the core complex area, as suggested in Figures 15a and 15b. A laterally limited body of migmatites might be the initial cause for strain localization to occur on the crustal scale, allowing core complex-type extension to develop [*Brun et al.,* 1994; *Tirel et al.,* 2004, 2006]. In addition, isothermal decompression of lower crustal rocks due to rapid exhumation at the apex of the core complex may result in a focused secondary anatexis [e.g., *Teyssier et al.,* 2005]. The latter process may account for seemingly continuous migmatization beneath the apex of the

Niğde core complex during at least 9 Ma while shallower parts of the dome underwent fast cooling (see section 7.2). In the following, we describe the scenario of Figures 15a and 15b and show how the interaction between lateral underflow and down-dip shearing along the detachment should result in a superposition of distinct structural domains within the migmatitic part of the core complex (Figure 15c). The observed counterparts in the Nigde dome are also discussed.

At early stage of extension, at ca. 84 Ma, the top of the nascent migmatite dome recorded pervasive top-to-ENE ductile shearing along the deeper segment of the detachment zone (Figure 15a). With ongoing exhumation, until ca. 76 Ma, ductile shearing became more localized. Therefore, in a late configuration, this part of the migmatite dome forms a cap having recorded intense top-to-ENE shearing along the detachment zone (Figure 15c). The cap coincides with the eastern slice of Gümüşler formation in Figures 2 and 3b, showing relictic migmatitic textures (Figures 9a and 11c). Beneath this cap, three superposed structural domains can be distinguished within the migmatite dome (Figure 15c). The lowermost one, approximately bounded by the 650°C isothermal surface, is the domain with current anatexis. Channel flow is expected to occur at this level. In the overlying domain, which represents the upper wall of the channel, top-to-SSW shearing (rotated to top-to-SSE shearing at deeper levels if underflow is strictly orthogonal) develops as a by-product of channel flow, assuming the latter proceeds preferably northward (see next section). Because top-to-SSW shearing is not recorded at temperatures lower than about 450°C, the corresponding isothermal surface is taken as the upper boundary of this intermediate domain. This highlights the fact that the influence of underflow on the active strain pattern is restricted to the most ductile part of the crust. Above the ~450°C isothermal surface, the third structural domain represents the "frozen" part of the migmatite dome, in which rocks have been exhumed too much to go on recording lateral underflow. As a result, earlier top-to-SSW ductile shearing is replaced by limited top-to-NE extensional faulting synthetic with the detachment, as seen in the core of the Niğde dome. This third domain is expected to appear as a distinct entity only after a significant amount of exhumation is achieved at the apex of the core complex (Figures 15b and 15c). In an earlier stage, while the top of the migmatite dome is still in the ductile part of the crust (Figure 15a), there should be a direct upward transition from active underflow to active ductile shearing along the deeper segment of the detachment zone. This might not be the case at the initiation of extension if the detachment is to form a continuous shear zone only after a certain amount of exhumation is achieved [*Tirel et al.,* 2004] (see section 5.2.1). Because denudation has been limited in the Niğde Massif since the end of core complex-type

extension, only the "cap" and "frozen" parts of the migmatite dome are exposed at present (Figure 3b).

7.3.3. Local Inward Flow vs. Regional Channel Flow

Lateral underflow may have developed on a relatively local scale, as a result of "inward" flow toward the core complex in a context of highly localized extension in the middle and upper crust [*Block and Royden,* 1990; *Wernicke,* 1990; *Wdowinski and Axen,* 1992; *Brun and Van den Driessche,* 1994; *Tirel et al.,* 2004]. Because flow is lateral, some material is expected to be added to a section parallel to the direction of extension and crossing the core complex, so that such a section would increase its surface area. As a consequence, lateral underflow may help to maintain the crust thicker in the vicinity of the core complex. This is illustrated in Figure 15b through a relative increase in Moho depth of about 5 km in the case the surface occupied by the migmatite dome is added. In Figures 15a and 15b, the horizontal distance across which crustal extension is homogeneous is taken at about twice the basal width of the core complex, assuming this is the distance over which lower crustal flow acts to balance localized extension in the upper crust [e.g., *Wernicke,* 1990]. Slightly greater distances are also possible [e.g., *Wdowinski and Axen,* 1992; *Tirel et al.,* 2004], which would result in a lower relative increase in Moho depth. The fact that underflow is dominantly lateral implies greater distances of transport in this direction, relative to those in the direction parallel to extension. Therefore, on the scale of a section constructed under the assumption of homogeneous deformation in the direction of extension, lateral inward flow should indeed result in a net addition of material.

As an alternative to inward flow on the scale of the core complex, lateral underflow may have developed on a larger scale, due to regional variations in crustal thickness [e.g., *Kruse et al.,* 1991; *Teyssier et al.,* 2005]. As discussed by *Gautier et al.* [2002], Latest Cretaceous high-magnitude extension probably affected the whole CACC [see also *Dirik et al.,* 1999; *Okay and Tüysüz,* 1999]. If the direction of extension maintained a ~E-W trend over the area, then the triangular shape of the CACC may suggest that the amount of extension has been greater in the northern part of the complex (Figure 15d). In this case, regional-scale channel flow would proceed northward, so as to compensate greater thinning there. This means that, in Figure 15b, some material would flow out of the plane of view (and not into it, as in the hypothesis of inward flow), resulting in a crust even thinner than in the case of plane strain deformation. North-directed channel flow is expected to result in top-to-south shearing along the upper wall of the channel, in agreement with the observed kinematics in the core of

the Niğde dome. The advantage of this interpretation is that it accounts for the record of non-coaxial deformation with a consistent sense of shear in the core of the dome. In contrast, convergent inward flow toward the dome apex should result in coaxial strain there.

The elliptical shape of most core complexes, including the Niğde dome (Figures 4 and 5), may even suggest that pure inward flow should result in a markedly divergent pattern of stretching lineations within the layer recording the flow. We are not aware of such an example in the literature, except possibly in the Ruby Mountains core complex (see below). Conceptual models and numerical simulations that include lower crustal flow being purely two-dimensional, it is difficult to anticipate how inward flow would occur in a three-dimensional setting. Nevertheless, we can assume that flow proceeds so as to minimize the transport of viscous material into the dome. If so, inward flow should occur preferentially in a direction parallel to extension in the case of elliptical core complexes with a long axis perpendicular to extension, which is the most common situation. As a fact, colinear lineations associated with down-dip shearing on either side of a core complex is a relatively common feature that may be interpreted as reflecting inward flow parallel to extension [*Gautier and Brun,* 1994], although there are other possible explanations. This interpretation seems particularly appropriate when the "bivergent" core complex includes weak lithologies (e.g., migmatites) and retains a pronounced asymmetry (that is, only one side of the core complex exposes a true detachment, the other side recording inward flow). The Velay migmatite dome, French Massif Central, provides a good example of this case [*Lagarde et al.,* 1994]. Lineations in the rearmost part of this subcircular dome display a concentric pattern which, together with the steeply overturned attitude of foliations, is explained by the rise and lateral expansion of the core diatexites. Bivergent extension in the rest of the dome is associated with lineations with a fairly constant trend [*Lagarde et al.,* 1994], and no divergent pattern is observed. In migmatites-bearing elliptical core complexes with a long axis parallel to extension, like on the Cyclades islands of Naxos and Paros, lineations within and around the migmatite core remain parallel to extension [*Gautier et al.,* 1993]. This seems contradictory with the above assumption of flow proceeding so as to minimize the transport of viscous material. Taken together, these features suggest that pure inward flow tends to occur preferably in a direction parallel to extension, regardless of the shape of the core complex. This, in turn, suggests that lateral underflow, when present, is more likely to reflect regional-scale channel flow due, e.g., to lateral variations in the amount of extension, as proposed here for the CACC. Interestingly, the same interpretation was given by *MacCready et al.* [1997] for the origin of lateral underflow in the Ruby Mountains core complex.

Finally, the two processes (local inward flow and regional channel flow) are not mutually exclusive and may operate together. The Ruby Mountains core complex also illustrates this point. At the same stuctural level where lateral underflow is recorded, large asymmetric fold nappes occur, with hinge lines orthogonal to the direction of extension. The two main nappes overlap and verge oppositely, a feature that *MacCready et al.* [1997] interpret as reflecting mid-crustal convergent flow toward the apex of the core complex. The nappes may therefore reflect extension-parallel inward flow developed concurrently with orthogonal regional-scale flow. In map view, stretching lineations within the level encompassing the nappes display a markedly divergent pattern. Given that this variation in lineation trend occurs at constant structural level (i.e., it does not relate to the progressive rotation of the lineation with depth), the divergent pattern indeed supports the hypothesis of combined extension-parallel inward flow and orthogonal regional flow [*MacCready et al.*, 1997]. That the two processes may operate together is not a surprise, as highly localized core complex-type extension and high-magnitude regional extension are frequently associated in continental areas involving a thermally weakened crust (see, e.g., *Tirel et al.* [2006] for a discussion of classical examples, and *Meng* [2003] for the recently identified but significant case of northeastern Asia).

7.4. Alternative Interpretation: Synmetamorphic Thrusting

An alternative interpretation for oblique shearing in the core of the Niğde dome involves synmetamorphic thrusting (Figures 15e and 15f). The most obvious support for this interpretation is the observed top-to-SSW sense of shear, because it coincides with the expected kinematics for regional-scale thrusting in this part of the Alpine orogen [*Görür et al.,* 1984; *Dirik et al.,* 1999; *Okay and Tüysüz,* 1999; *Floyd et al.,* 2000; *Kaymakci,* 2000]. In this case, top-to-NE/ENE extensional shearing at higher levels of the dome would reflect syn-thrusting extension. The high obliquity between the two shearing events would be consistent with the picture of syn-thickening extension, as seen in other orogens [e.g., *Tapponnier et al.,* 1981; *Gapais et al.,* 1992]. Despite its attractive simplicity, however, the following discussion precludes us from favouring this interpretation. A key observation is that much of the top-to-SSW shearing deformation in the core of the dome is recorded after migmatization (Figures 7c and 7d). Therefore, the horizon across which strain partitioning has occurred (from top-to-SSW shearing, below, to top-to-NE/ENE shearing, above) does not lie within the part of the migmatite dome with current anatexis, but above it, as illustrated in Figure 15c. Assuming top-to-SSW shearing reflects thrusting, this would imply that the anatectic layer lies within

the thrust zone while the transition to simultaneous extension occurs higher in the colder metamorphic pile (Figure 15e). We consider unlikely such a situation where the weakest layer in the metamorphic pile would not have been used as the horizon for decoupling thrusting from overlying extension, given the observations in the Himalayan type case [e.g., *Gapais et al.,* 1992; *Searle et al.,* 1997; *Grujic et al.,* 2002] and the results of numerical models simulating syn-thickening extension in the presence of a weak lower crust [*Beaumont et al.,* 2001].

The above argument should especially apply in cases where the thickness of the weak layer (migmatites or/and syn-kinematic intrusions) is large (>0.5-1 km), as in typical sections documenting coeval thrusting and extension across the Higher Himalaya Crystalline [*Gapais et al.,* 1992; *Searle et al.,* 1997; *Vannay and Grasemann,* 2001]. Evidence was given in section 7.2 that the body of migmatites seen in the core of the Niğde dome extends downward for at least 5 km, thus apparently fitting the condition of a thick weak layer. However, starting from ca. 82 Ma, not the whole of this pile was anatectic, as the exposed migmatites were already cooler than 650°C. Migmatization at greater depth is known only through the emplacement of younger intrusions, until ca. 76 Ma. Therefore, at a given time, the thickness of the current anatectic body could have been less than 5 km. This would imply that anatexis moved progressively downward with respect to the rock pile or/and rocks moved upward with respect to a constant depth range for anatexis. Decompression melting beneath the apex of the core complex [e.g., *Teyssier et al.,* 2005] could, in principle, account for this behavior. However, we doubt this could have involved an anatectic layer both thinner than 0.5-1 km and migrating vertically for more than 4-5 km, as this would imply that each rock experienced partial melting during only a small fraction of the period from 85 to 76 Ma. Figure 15e depicts a situation commonly met with higher-grade synmetamorphic thrusts, in which anatexis is restricted to the hangingwall unit, or penetrates the footwall unit only near its top. Transposed to the Niğde dome, this scenario would imply that much, if not all, of the >5 km-thick pile of migmatites lies in the hangingwall of a major thrust. In such a situation, the cooling effect of underthrusting is expected to act against the downward migration of anatexis. If so, much of the migmatitic pile should have existed from the beginning, forming a thick anatectic body that progressively thinned through cooling of its upper parts. Therefore, in the context of the synmetamorphic thrust hypothesis, the prolonged existence of a weak layer of significant thickness (>0.5-1 km) seems the most plausible solution. This, in turn, leads us not to favor this hypothesis, as stated above. Nevertheless, we do not rule it out, keeping in mind that

synmetamorphic thrusting may involve more complex relations between thrusts and anatexis (e.g., out-of-sequence thrusting within the migmatitic pile [*Grujic et al.,* 2002]).

8. Late-Stage Exhumation and Formation of the Ulukışla Basin

The Ulukışla Basin bounds the Niğde Massif to the south (Figures 1 and 2) and part of its sedimentary sequence is subcontemporaneous with the exhumation of the metamorphic rocks (Figure 14), therefore the relations between the core complex and the basin deserve special attention. The temperature-time path drawn in Figure 14 follows the proposal of *Gautier et al.* [2002], according to which lower unit rocks reached the surface after the deposition of the late Maastrichtian to Late Paleocene sediments (see section 2.3). If so, these sediments accumulated during the exhumation of the metamorphic dome. Then, it is tempting to interpret them as the infill of one or several half-grabens associated with the major NE/ENE-dipping detachment identified in the massif [*Gautier et al.,* 2002]. Because it lies essentially to the southwest of the dome, the Ulukışla Basin itself could be viewed either as an early supra-detachment basin left behind the rising dome, in a model involving pronounced arching of the detachment fault [e.g., *Lister and Davis,* 1989], or as a half-graben associated with a major normal fault developed at the rear of the detachment-core complex system (the "listric accommodation fault" of *Brun et al.* [1994]). However, both hypotheses seem inadequate, because the earliest sediments (late Maastrichtian) were deposited while much of the cooling and, therefore, much of the exhumation of the dome had already occurred (Figure 14). In addition, there is no evidence for a major north-dipping normal fault zone in the southern part of the basin. Along its southern margin, despite later folding and thrusting, the unconformity of the late Maastrichtian deposits over earlier structures of the Taurides is still visible [e.g., *Clark and Robertson,* 2002]. Thus, the opening of the Ulukışla Basin was probably a late event, unrelated to shearing along the NE/ENE-dipping detachment.

At the time of the earliest deposits, lower unit rocks were already cooler than 300°C (Figure 14), hence any deformation would have been brittle. Our observations show that, following top-to-NE ductile shearing, the southwestern margin of the dome has recorded ongoing NE-SW stretching in brittle conditions (Figure 12e) together with, or followed by, roughly top-to-south shearing along a series of brittle shear zones developed within quartzites and minor marbles (Figures 12c and 12d) (see section 3.4). We tentatively interpret these features as reflecting the temporal transition from top-to-NE shearing during detachment-type extension (Figure 15b) to down-dip shearing along a newly formed south-dipping normal fault zone following the southern flank of the core complex (Figures 15g and 15h). The low-

dipping normal fault bounding this part of the dome (Figures 2 and 5), described as a detachment by *Whitney and Dilek* [1997] and *Fayon et al.* [2001], may well belong to this secondary fault system. While part of the displacement along the fault is probably Neogene [*Gautier et al.,* 2002], some of the grooves and striations on it, especially those trending approximately north-south (Figure 5), might date from the tectonic stage shown in Figure 15g. Because the Ulukışla Basin lies immediately to the south, we interpret the Maastrichtian-Paleocene part of the sedimentary sequence as the infill of a large graben in the hangingwall of the south-dipping normal fault system (Figures 15g and 15h). For simplicity, Figures 15b and 15g show a similar geometry for the dome, so that the corresponding time interval does not seem to have included any exhumation of the metamorphic rocks (this is because Figure 15b shows the section as if the detachment accommodated all the exhumation). However, considering that the Maastrichtian-Paleocene sediments were probably deposited while the metamorphic rocks were still on their way to the surface (Figure 14), a minimum amount of exhumation should be attributed to shearing along the south-dipping fault system. This happened while the metamorphic rocks were cooler than about 300°C (see section 3.4). Therefore, taking a geothermal gradient of at least 30°C/km, this second-stage exhumation accommodated less than 10 km of vertical displacement. The Maastrichtian-Paleocene sediments of the Tuzgölü Basin (Figure 15h) probably connect with the Ulukışla Basin beneath a blanket of younger deposits [*Görür et al.,* 1984]. They may have formed in the same context of ongoing, or renewed, extension on the margins of the CACC (Figure 15h), following high-magnitude/core complex-type extension within the CACC (Figure 15d). In the Niğde area, the first period of extension ended later than 76.8 Ma (see section 6). The second period of extension followed, with or without an interlude, or eventually with a brief overlap. It ended sometimes in between 60 and 54 Ma, i.e., before the onlap of nonconformable Eocene sediments (Figure 14), considering that a significant change in tectonic environment occurred at around that time (see section 2.3).

9. Conclusions

The main results of this study are as follows:

1. Two structural units are distinguished in the Niğde Massif, the upper unit having experienced significantly lower peak conditions of metamorphism than the lower unit has. Foliations and lithological contours in the lower unit define a broad dome having gently dipping slopes and a core dominated by metatexitic migmatites.

2. The contact between the two units bears all the structural elements of a ductile to brittle extensional detachment. Therefore, the Niğde metamorphic dome represents a typical extensional core complex. Top-to-NE/ENE shearing at higher levels of the lower unit reflects displacement along the detachment zone, whose initial dip is estimated to be about 40°. Deeper levels of the lower unit display top-to-SSW ductile shearing that was active during and after migmatization, followed by limited top-to-NE/NNE semi-brittle to brittle shearing. The two shearing deformations (top-to-NE/ENE at higher levels vs. top-to-SSW at deeper levels) are oblique in the horizontal plane, with the difference in the mean trend of stretching lineations reaching 58°. The sharp transition between the two deformations lies within the migmatitic part of the dome.

3. Geochronological data indicate that the two shears were active together while lower unit rocks experienced temperatures around 500°C, reflecting a process of strain partitioning in the lower-middle crust. The data also yield a mean cooling rate of about 60°C/Ma during cooling of lower unit rocks from ~700 to ~300°C, consistent with the record in other extensional core complexes. Structural and radiometric data on the migmatites and granitoids of crustal origin suggest that the body of migmatites seen in the core of the dome has a downward extent of at least 5 km. Migmatization was maintained beneath the apex of the core complex for at least 9 Ma, from ca. 85 to 76 Ma, while the shallower parts of the dome were undergoing fast cooling.

4. Oblique shearing in the core of the Niğde dome is interpreted as reflecting lateral underflow, i.e., horizontal flow of the lower crust in a direction orthogonal or highly oblique to the direction of extension, in a context of core complex-type and/or high-magnitude regional-scale extension. As a result of the interaction between lateral underflow and down-dip shearing along the overlying detachment, four superposed structural domains should exist within the migmatitic part of the core complex once earlier exhumation has brought the topmost migmatites in the field of brittle deformation. From bottom to top, these are (1) the domain with contemporaneous anatexis, in which channel flow is expected to occur, (2) the upper wall of the channel, characterized by non-coaxial deformation, illustrated by top-to-SSW shearing in the core of the Niğde dome, (3) the “frozen” domain, in which rocks have been exhumed too much to continue recording lateral underflow, so that earlier ductile shearing is replaced by limited brittle shearing synthetic with the detachment, and (4) the topmost migmatites, which have recorded ductile then brittle shearing along the detachment zone, illustrated by top-to-NE/ENE shearing in the envelope of the Niğde dome. Because

denudation has been limited since extension ceased, only domains (3) and (4) are exposed at present. Structural data suggest that the boundary between domains (2) and (3) coincides approximately with the 450°C isothermal surface, which highlights the fact that the influence of underflow on the active strain pattern is restricted to the most ductile part of the crust.

5. Lateral underflow may reflect inward flow on the scale of the core complex, or channel flow on a regional scale. The latter has the advantage of explaining the record of non-coaxial deformation in the core of the Niğde dome. More generally, we suspect that the development of lateral underflow in a core complex more likely reflects regional channel flow, rather than local inward flow.

6. A possible alternative interpretation for oblique shearing in the core of the Niğde dome involves synmetamorphic thrusting, as top-to-SSW shearing fits with the expected kinematics for regional-scale thrusting in this part of the Alpine orogen. Top-to-NE/ENE extensional shearing at higher levels of the dome would then reflect syn-thrusting extension. Nevertheless, we do not favor this interpretation.

7. Following core complex-type extension, which vanished later than 77 Ma, a south-dipping normal fault zone developed along the southern flank of the Niğde dome. It contributed to the latest <10 km of denudation of the lower unit rocks. Late Maastrichtian-Paleocene sediments of the Ulukışla Basin are interpreted as the infill of a large graben in the hangingwall of this secondary fault system. The Ulukışla Basin and the contemporaneous Tuzgölü Basin probably formed in the same context of ongoing, or renewed, extension on the margins of the CACC, following high-magnitude/core complex-type extension within the CACC. This second period of extension ended sometimes in between 60 and 54 Ma, before the onlap of nonconformable Eocene sediments onto the high-grade rocks of the CACC.

Acknowledgments. This study was supported by a CNRS-TÜBITAK Cooperation Program (projects 7166 and 8037). We are indebted to the Turkish Scientific and Technical Research Council which funded the field work (Project TÜBITAK YDABÇAG 100Y030). Olivier Vanderhaeghe and Roli Oberhänsli are thanked for their careful reviews.

References

Akıman, O., A. Erler, M. C. Göncüoğlu, N. Güleç, A. Geven, T. K. Türeli, and Y. K. Kadıoğlu (1993), Geochemical characteristics of granitoids along the western margin of the Central Anatolian Crystalline Complex and their tectonic implications, *Geol. J.*, *28*, 371-382.

Amato, J. M., and E. L. Miller (2004), Geological map and summary of the evolution of the Kigluaik Mountains

gneiss dome, Seward Peninsula, Alaska, in *Gneiss Domes in Orogeny*, edited by D. L. Whitney, C. Teyssier and C. S. Siddoway, *Spec. Pap. Geol. Soc. Am.*, *380*, 295-306.

Anders, M. H., E. Aharonov, and J. J. Walsh (2000), Stratified granular media beneath large slide blocks: Implications for mode of emplacement, *Geology*, *28*, 971-974.

Andronicos, C. L., D. H. Chardon, L. S. Hollister, G. E. Gehrels, and G. J. Woodsworth (2003), Strain partitioning in an obliquely convergent orogen, plutonism, and synorogenic collapse: Coast Mountains Batholith, British Columbia, Canada, *Tectonics*, *22*(2), 1012, doi: 10.1029/2001TC001312.

Arnaud, N. O., M. Brunel, J. M. Cantagrel, and P. Tapponnier (1993), High cooling and denudation rates at Kongur Shan, Eastern Pamir (Xinjiang, China) revealed by $^{40}Ar/^{39}Ar$ alkali feldspar thermochronology, *Tectonics, 12,* 1335-1346.

Beaumont, C., R. A. Jamieson, M. H. Nguyen, and B. Lee (2001), Himalayan tectonics explained by extrusion of a low-viscosity crustal channel coupled to focused surface denudation, *Nature*, *414*, 738-742.

Berthé, D., P. Choukroune, and P. Jegouzo (1979), Orthogneiss, mylonite and non-coaxial deformation of granites : The example of the South Armorican Shear Zone, *J. Struct. Geol., 1,* 31-42.

Block, L., and L. H. Royden (1990), Core complex geometries and regional scale flow in the lower crust, *Tectonics*, *9*, 557-567.

Brun, J. P., and J. Van den Driessche (1994), Extensional gneiss domes and detachment fault systems: Structure and kinematics, *Bull. Soc. Géol. France*, *165*, 519-530.

Brun, J. P., D. Sokoutis, and J. Van den Driessche (1994), Analogue modeling of detachment fault systems and core complexes, *Geology*, *22*, 319-322.

Buck, W. R. (1991), Modes of continental lithospheric extension, *J. Geophys. Res.*, *96*, 20,161-20,178.

Clark, M., and A. H. F. Robertson (2002), The role of the Early Tertiary Ulukışla Basin, southern Turkey, in suturing of the Mesozoic Tethys ocean, *J. Geol. Soc. London*, *159*, 673-690.

Dallmeyer, R. D., A. W. Snoke, and E. H. McKee (1986), The Mesozoic-Cenozoic tectonothermal evolution of the Ruby Mountains, East Humboldt Range, Nevada: A cordilleran metamorphic core complex, *Tectonics*, *5*, 931-954.

Dinçer, F., and N. Avşar (2004), Çamardı (Niğde) yöresi Tersiyer (Lütesiyen) sedimanlarının bentik foraminifer biyostratigrafisi, *Hacettepe Üniversitesi Yerbilimleri Uygulama ve Araştırma Merkezi Bülteni*, *30*, 35-48.

Dirik, K., M. C. Göncüoğlu, and H. Kozlu (1999), Stratigraphy and pre-Miocene tectonic evolution of the southwestern part of the Sivas Basin, Central Anatolia, Turkey, *Geol. J.*, *34*, 303-319.

Fayon, A. K., D. L. Whitney, C. Teyssier, J. I. Garver, and Y. Dilek (2001), Effects of plate convergence obliquity on timing and mechanisms of exhumation of a mid-crustal terrain, the Central Anatolian Crystalline Complex, *Earth Planet. Sci. Lett.*, *192*, 191-205.

Floyd, P. A., M. C. Göncüoğlu, J. A. Winchester, and M. K. Yalınız (2000), Geochemical character and tectonic environment of Neotethyan ophiolitic fragments and metabasites in the Central Anatolian Crystalline Complex, Turkey, in *Tectonics and Magmatism in Turkey and the Surrounding Area*, edited by E. Bozkurt, J. A. Winchester and J. D. A. Piper, *Geol. Soc. Spec. Publ.*, *173*, 183-202.

Gapais, D. (1989), Shear structures within deformed granites: Mechanical and thermal indicators, *Geology*, *17*, 1144-1147.

Gapais, D., A. Pêcher, E. Gilbert, and M. Ballèvre (1992), Synconvergence spreading of the Higher Himalaya Crystalline in Ladakh, *Tectonics*, *11*, 1045-1056.

Gautier, P., and J. P. Brun (1994), Ductile crust exhumation and extensional detachments in the central Aegean (Cyclades and Evvia islands), *Geodin. Acta*, *7*, 57-85.

Gautier, P., J. P. Brun, and L. Jolivet (1993), Structure and kinematics of Upper Cenozoic extensional detachment on Naxos ans Paros (Cyclades Islands, Greece), *Tectonics*, *12*, 1180-1194.

Gautier, P., E. Bozkurt, E. Hallot, and K. Dirik (2002), Dating the exhumation of a metamorphic dome: Geological evidence for pre-Eocene unroofing of the Niğde Massif (Central Anatolia, Turkey), *Geol. Mag.*, *139*, 559-576.

Göncüoğlu, M. C. (1986), Geochronological data from the southern part (Niğde area) of the Central Anatolian Massif, *Bulletin of the Mineral Research and Exploration Institute of Turkey (MTA)*, *105/106*, 83-96.

Göncüoğlu, M. C., V. Toprak, I. Kuşcu, A. Erler, and E. Olgun (1991), Orta Anadolu Masifinin batı bölümünün jeolojisi, Bölüm 1: Güney Kesim, *Turkish Petroleum Corporation (TPAO) Report*, *2909*, 140 pp.

Görür, N., F. Y. Oktay, I. Seymen, and A. M. C. Şengör (1984), Palaeotectonic evolution of the Tuzgölü basin complex, Central Turkey: Sedimentary record of a Neo-Tethyan closure, in *The Geological Evolution of the Eastern Mediterranean*, edited by J. E. Dixon and A. H. F. Robertson, *Geol. Soc. Spec. Publ.*, *17*, 467-482.

Grujic, D., L. S. Hollister, and R. R. Parrish (2002), Himalayan metamorphic sequence as an orogenic channel: Insight from Bhutan, *Earth Planet. Sci. Lett.*, *198*, 177-191.

Ilbeyli, N. (2005), Mineralogical-geochemical constraints on intrusives in central Anatolia, Turkey: Tectono-magmatic evolution and characteristics of mantle source, *Geol. Mag.*, *142*, 187-207.

Jaffey, N., and A. H. F. Robertson (2001), New sedimentological and structural data from the Ecemiş Fault Zone, southern Turkey: Implications for its timing and offset and the Cenozoic tectonic escape of Anatolia, *J. Geol. Soc. London*, *158*, 367-378.

Jolivet, L., O. Beyssac, B. Goffé, D. Avigad, C. Lepvrier, H. Maluski, and T. Ta Trong (2001), Oligo-Miocene midcrustal subhorizontal shear zone in Indochina, *Tectonics*, *20*, 46-57.

Jolivet, L., V. Famin, C. Mehl, T. Parra, C. Aubourg, R. Hébert, and P. Philippot (2004), Strain localization during crustal-scale boudinage to form extensional metamorphic domes in the Aegean Sea, in *Gneiss Domes in Orogeny*, edited by D. L. Whitney, C. Teyssier and C. S. Siddoway, *Spec. Pap. Geol. Soc. Am.*, *380*, 185-210.

Kadıoğlu, Y. K., Y. Dilek, N. Güleç, and K. A. Foland (2003), Tectonomagmatic evolution of bimodal plutons in the Central Anatolian Crystalline Complex, Turkey, *J. Geol.*, *111*, 671-690.

Kaymakci, N. (2000), Tectono-stratigraphical evolution of the Çankırı Basin (Central Anatolia, Turkey), Ph.D. thesis, Univ. Utrecht, The Netherlands, *Geologica Ultraiectina, 190,* 247 pp.

Kirschner, D. L., M. A. Cosca, H. Masson, and J. C. Hunziker (1996), Staircase $^{40}Ar/^{39}Ar$ spectra of fine-grained white mica: Timing and duration of deformation and empirical constraints on argon diffusion, *Geology*, *24*, 747-750.

Koçyiğit, A., and A. Beyhan (1998), A new intracontinental transcurrent structure: The Central Anatolian Fault Zone, Turkey, *Tectonophysics, 284,* 317-336.

Köksal, S., R. L. Romer, M. C. Göncüoğlu, and F. Toksoy-Köksal (2004), Timing of post-collisional H-type to A-type granitic magmatism: U-Pb titanite ages from the Alpine central Anatolian granitoids (Turkey), *Int. J. Earth Sci.*, *93*, 974-989.

Kruse, S., M. McNutt, J. Phipps-Morgan, L. Royden, and B. Wernicke (1991), Lithospheric extension near Lake Mead, Nevada: A model for ductile flow in the lower crust, *J. Geophys. Res., 96,* 4435-4456.

Lagarde, J. L., C. Dallain, P. Ledru, and G. Courrioux (1994), Strain patterns within the late Variscan granitic dome of Velay, French Massif Central, *J. Struct. Geol.*, *16*, 839-852.

Leloup, P. H., R. Lacassin, P. Tapponnier, U. Schärer, D. Zhong, X. Liu, L. Zhang, S. Ji, and T. Phan Trong (1995), The Ailao Shan-Red River shear zone (Yunnan, China), Tertiary transform boundary of Indochina, *Tectonophysics*, *251*, 3-84.

Lister, G. S., and G. A. Davis (1989), The origin of metamorphic core complexes and detachment faults formed during Tertiary continental extension in the northern Colorado River region, U.S.A., *J. Struct. Geol.*, *11*, 65-94.

MacCready, T., A. W. Snoke, J. E. Wright, and K.A.Howard (1997), Mid-crustal flow during Tertiary extension in the Ruby Mountains core complex, Nevada, *Geol. Soc. Am. Bull.*, *109*, 1576-1594.

McKenzie, D., F. Nimmo, J. A. Jackson, P. B. Gans, and E. L. Miller (2000), Characteristics and consequences of flow in the lower crust, *J. Geophys. Res.*, *105*, 11,029-11,046.

Mehl, C., L. Jolivet, and O. Lacombe (2005), From ductile to brittle: Evolution and localization of deformation below a crustal detachment (Tinos, Cyclades, Greece), *Tectonics*, *24*, TC4017, doi: 10.1029/2004TC001767.

Meng, Q. R. (2003), What drove late Mesozoic extension of the northern China-Mongolia tract?, *Tectonophysics*, *369*, 155-174.

Okay, A. I., and O. Tüysüz (1999), Tethyan sutures of northern Turkey, in *The Mediterranean Basins: Tertiary Extension within the Alpine Orogen*, edited by B. Durand, L. Jolivet, F. Horvath and M. Séranne, *Geol. Soc. Spec. Publ.*, *156*, 475-515.

Schmitz, M. D., and S. A. Bowring (2001), U-Pb zircon and titanite systematics of the Fish Canyon Tuff: An assessment of high-precision U-Pb geochronology and its application to young volcanic rocks, *Geochim. Cosmochim. Acta*, *65*, 2571-2587.

Searle, M. P., R. R. Parrish, K. V. Hodges, A. Hurford, M. W. Ayres, and M. J. Whitehouse (1997), Shisha Pangma leucogranite, South Tibetan Himalaya: Field relations, geochemistry, age, origin, and emplacement, *J. Geol.*, *105*, 295-317.

Simpson, C. (1985), Deformation of granitic rocks across the brittle-ductile transition*, J. Struct. Geol., 7,* 503-511.

Tapponnier, P., J. L. Mercier, R. Armijo, H. Tonglin, and Z. Ji (1981), Field evidence for active normal faulting in Tibet, *Nature*, *294*, 410-414.

Teyssier, C., E. C. Ferré, D. L. Whitney, B. Norlander, O. Vanderhaeghe, and D. Parkinson (2005), Flow of partially molten crust and origin of detachments during collapse of the Cordilleran Orogen, in *High-Strain Zones: Structure and Physical Properties*, edited by D. Bruhn and L. Burlini, *Geol. Soc. Spec. Publ.*, *245*, 39-64.

Tirel, C., J. P. Brun, and E. Burov (2004), Thermo-mechanical modeling of extensional gneiss domes, in *Gneiss Domes in Orogeny*, edited by D. L. Whitney, C. Teyssier and C. S. Siddoway, *Spec. Pap. Geol. Soc. Am.*, *380*, 67-78.

Tirel, C., J. P. Brun, and D. Sokoutis (2006), Extension of thickened and hot lithospheres: Inferences from laboratory modeling, *Tectonics*, *25*, TC1005, doi: 10.1029/2005TC001804.

Toprak, V., and M. C. Göncüoğlu (1993), Tectonic control on the development of the Neogene-Quaternary Central Anatolian Volcanic Province, Turkey, *Geol. J.*, *28*, 357-369.

Vanderhaeghe, O., C. Teyssier, I. McDougall, and W. J. Dunlap (2003), Cooling and exhumation of the Shuswap Metamorphic Core Complex constrained by $^{40}Ar/^{39}Ar$ thermochronology, *Geol. Soc. Am. Bull.*, *115*, 200-216.

Vannay, J. C., and B. Grasemann (2001), Himalayan inverted metamorphism and syn-convergence extension as a consequence of a general shear extrusion, *Geol. Mag.*, *138*, 253-276.

Wdowinski, S., and G. J. Axen (1992), Isostatic rebound due to tectonic denudation: A viscous flow model of a layered lithosphere, *Tectonics*, *11*, 303-315.

Wernicke, B. P. (1990), The fluid crustal layer and its implications for continental dynamics, in *Exposed Cross-Sections of the Continental Crust*, edited by M. H. Salisbury and D. M. Fountain, *NATO ASI Ser. C*, *317*, 509-544.

Whitney, D. L., and Y. Dilek (1997), Core complex development in central Anatolia, Turkey, *Geology*, *25*, 1023-

1026.

Whitney, D. L., and Y. Dilek (1998), Metamorphism during Alpine crustal thickening and extension in Central Anatolia, Turkey: The Niğde metamorphic core complex, *J. Petrology*, *39*, 1385-1403.

Whitney, D. L., C. Teyssier, Y. Dilek, and A. K. Fayon (2001), Metamorphism of the Central Anatolian Crystalline Complex, Turkey: Influence of orogen-normal collision vs. wrench-dominated tectonics on P-T-t paths, *J. Metamorph. Geol.*, *19*, 411-432.

Whitney, D. L., C. Teyssier, A. K. Fayon, M. A. Hamilton, and M. Heizler (2003), Tectonic controls on metamorphism, partial melting, and intrusion: Timing and duration of regional metamorphism and magmatism in the Niğde Massif, Turkey, *Tectonophysics*, *376*, 37-60.

Yetiş, C., G. Kelling, S. L. Gökçen, and F. Baroz (1995), A revised stratigraphic framework for Later Cenozoic sequences in the northeastern Mediterranean region, *Geol. Rundsch.*, *84*, 794-812.

Figure captions

Figure 1. Simplified structural map showing the position of the study area in central Turkey. CACC, Central Anatolian Crystalline Massif.

Figure 2. Geological map of the Niğde Massif, simplified and modified after *Göncüoğlu et al.* [1991]. Ellipses and rectangles indicate the numbers of dated samples described in *Whitney et al.* [2003] and this work, respectively.

Figure 3. Two cross-sections through the Niğde Massif (see Figure 2 for location), with a summary of radiometric data from the literature (in italics, 'K-Ar data' from *Göncüoğlu* [1986], otherwise from *Whitney et al.* [2003]) and this work. Foliation planes in the migmatite dome are concordant with those in the metamorphic rocks (see Figure 4), all being concordant with lithological contacts. For convenience, Üçkapılı-type granitic intrusions are shown rooted at shallow levels of the migmatite dome, although most of them probably originate from significantly deeper levels.

Figure 4. Structural map of the Niğde Massif, displaying the orientation of foliation and stratification planes, with dips in degrees.

Figure 5. Structural map of the Niğde Massif, displaying the orientation of stretching lineations and striations, remarkable occurrences of tectonic breccias, and foliation trajectories in the western part of the massif (deduced from the data in Figure 4).

Figure 6. Field views in the upper unit. (a) Gabbro showing an unevenly developed mineral fabric crosscut by tonalitic veins with diffuse margins and no or slight internal fabric paralleling their walls; these features indicate that the fabrics are magmatic in origin. (b) Foliated gabbro within a meter-thick greenschist facies shear zone at the base of the upper unit. Lense cap is 5 cm in diameter.

Figure 7. Structures at deeper levels of the lower unit (see Figure 5 for location). (a) and (b) Metatexitic migmatites with cm to 10 cm-thick low angle shear bands along which the products of melting have been collected, documenting the synchronism between top-to-SSW shearing and migmatization. (c) and (d) Migmatites in which the leucosomes are tightly folded and transposed into parallelism with the external foliation; in (d), the foliation itself is bent into sigmoids by a set of low angle shear bands, indicating that top-to-SSW shearing went on after migmatization ended. (e) σ-type quartz-feldspar aggregate flanked by asymmetric elongated wings, attesting for penetrative top-to-SSW shearing.

Figure 8. Structures at deeper levels of the lower unit (see Figures 2 and 5 for location). (a) Landscape view (roadcut at the bottom left) on a series of NNE-dipping low-angle normal faults. The strike of the hill is at ~70° to the strike of the faults, hence apparent dips are almost true dips. (b) Meter-thick semi-brittle shear zone in migmatitic paragneisses, with marbles in the hangingwall. (c) Meter-thick granitic dike, from which sample N13 was taken, crosscutting the foliation of the host rocks; near the bottom of the view, the dike also crosscuts a dm-thick pegmatitic vein. (d) Photomicrograph in sample N13, showing details of the C-S fabric (see the text for a description). Plane-polarized light; base of view 3 mm. (e) Age spectrum obtained from $^{40}Ar/^{39}Ar$ dating of biotite population in sample N13.

Figure 9. Structures at higher levels of the lower unit (see Figure 5 for location). (a) example of site showing migmatitic layering tightly folded in between top-to-NE shear bands (the view faces toward the east); such sites are marked with a star on Figure 5. (b) NE-dipping ultracataclastic joints in the part of the main body of Üçkapılı granite that displays C-S fabrics (see Figure 8 of *Gautier et al.* [2002]); the view faces toward the north.

Figure 10. Two-mica granite, from which sample N16 was taken, showing a pervasive top-to-ENE C-S fabrics (see Figures 3b and 5 for location). (a) Field view of the fabric about 20 m below the roof of the intrusion. (b) Photomicrograph in sample N16, showing details of the C-S fabric; biotite and muscovite grains are aligned parallel to the fabric. Plane-polarized light; base of view 3 mm. (c) Age spectrum obtained from $^{40}Ar/^{39}Ar$ dating of muscovite population in sample N16.

Figure 11. Structures at higher levels of the lower unit, on a roadcut exposure about 50 m below the contact with the upper unit (see Figures 3b and 5 for location). (a) NE-dipping semi-brittle shear zones and steeper normal faults crosscutting the flat-lying mylonitic fabric of the metamorphic rocks (darker) and concordant granitic intrusions (lighter). (b) Close-up at the left end of view (a). (c) Mylonitic paragneiss with relictic migmatitic texture, in which asymmetric boudinage of a quartz-feldspar segregation documents penetrative top-to-NE

shearing. (d) Localized shear bands in the same lithology as in (c). (e) Photomicrograph of a σ-type feldspar porphyroclast in a mylonitized granitic intrusion. Crossed polars light; base of view 1.5 mm. (f) Photomicrograph in sample N44, a mylonitized leucocratic intrusion containing fine-grained synfolial muscovite and coarser asymmetric fish-type clasts. Crossed polars light; base of view 1.5 mm. (g) Age spectrum obtained from $^{40}Ar/^{39}Ar$ dating of muscovite population in sample N44.

Figure 12. Features associated with brittle deformation along the southern margin of the massif (see Figure 5 for location). (a) Outcrop showing Eocene conglomerates nonconformably overlying quartzites of the lower unit; a decimeter-thick steep ultracataclastic joint (in between arrows) crosscuts at right angle both the foliation and the NE-SW-trending stretching lineation of the quartzites. (b) Close-up of the nonconformity seen in (a), showing, from top to bottom, a conglomerate with subangular clasts, the rugged erosional surface defining the nonconformity (dashed line), and quartzites bearing by a decimeter-thick ultracataclastic joint (arrow), itself crosscut by the erosional surface. (c) Ferric oxi-hydroxides-rich reddish microbreccia displaying SSE-dipping laminations associated with grain-size grading. (d) Ferric oxi-hydroxides-rich purple microbreccia bearing well rounded quartzite clasts. (e) Granitic intrusion crosscut by numerous steep quartz veins with a regular NW-SE trend.

Figure 13. Additional $^{40}Ar/^{39}Ar$ data (see Figure 2 for location). (a) Photomicrograph in sample N8, showing that the linear/planar fabric in this amphibolite is defined primarily by the preferred orientation of amphibole grains. XZ section; plane-polarized light; base of view 3 mm. (b), (c) and (d) Age spectra obtained from $^{40}Ar/^{39}Ar$ dating of mineral populations in samples N8, N49 and N67, respectively (see the text for a description of the rocks). Vertical arrows in (b) highlight the boundaries between steps with almost identical values.

Figure 14. Temperature-time diagram synthesizing available radiometric and biostratigraphic data on the Niğde Massif. All radiometric data refer to the lower unit. Uncertainties in closure temperature are ± 50°C, except for argon in muscovite, for which we adopt ± 75°C (see the text). The dark grey box shows the bulk envelope of ages in the temperature range 250-575°C; the corresponding data are detailed in the enlargement (right). When available (that is, in the case for argon chronometers), ages from deeper vs. higher levels of the lower unit are plotted slightly above vs. below the mean closure temperature, respectively. Other chronometers relate to deeper levels only. For the sake of clarity, uncertainties in closure temperature are reduced to ± 25°C in the enlargement. In the left diagram, a temperature-time mean path is drawn together with a temperature-time "wider

band", in light grey, which includes all possible paths within the range of available data. Both the path and the band use data from deeper levels of the lower unit only.

Figure 15. Crustal-scale scenario for the tectonic evolution of the Niğde Massif during the Late Cretaceous. Sketches (e) and (f) represent an unfavored alternative to sketches (b) and (d). In both cases, the metamorphic dome represents a core complex developed in response to shearing along a major NE/ENE-dipping detachment. Sketch (c) depicts the vertical distribution of structural domains within the migmatitic part of the dome according to our favored interpretation, that is, considering top-to-SSW shearing in the core of the dome as reflecting lateral flowing of the lower crust during bulk crustal extension. In the alternative of (e) and (f), top-to-SSW shearing reflects synmetamorphic thrusting. The dotted line in (b) delineates the Moho in the hypothesis of plane strain deformation, that is, when the surface area is kept constant starting from the configuration (a). The amount of extension in (b) is deduced from the present geometry of the Niğde dome. Bulk crustal extension is assumed to be homogeneous over a distance twice the basal width of the core complex. This sets the horizontal length in (a) at 102 km, which, in turn, results in a Moho at 25.5 km in (b). The alternative Moho at 30 km is obtained when the surface occupied by the migmatite dome is added, assuming it corresponds to material flown from outside the plane of view, in the hypothesis where lateral underflow reflects "inward" flow on the scale of the core complex. Conversely, if lateral underflow reflects channel flow on a regional scale, as shown in (d), the crust in (b) should be thinner than in the case of plane strain deformation.

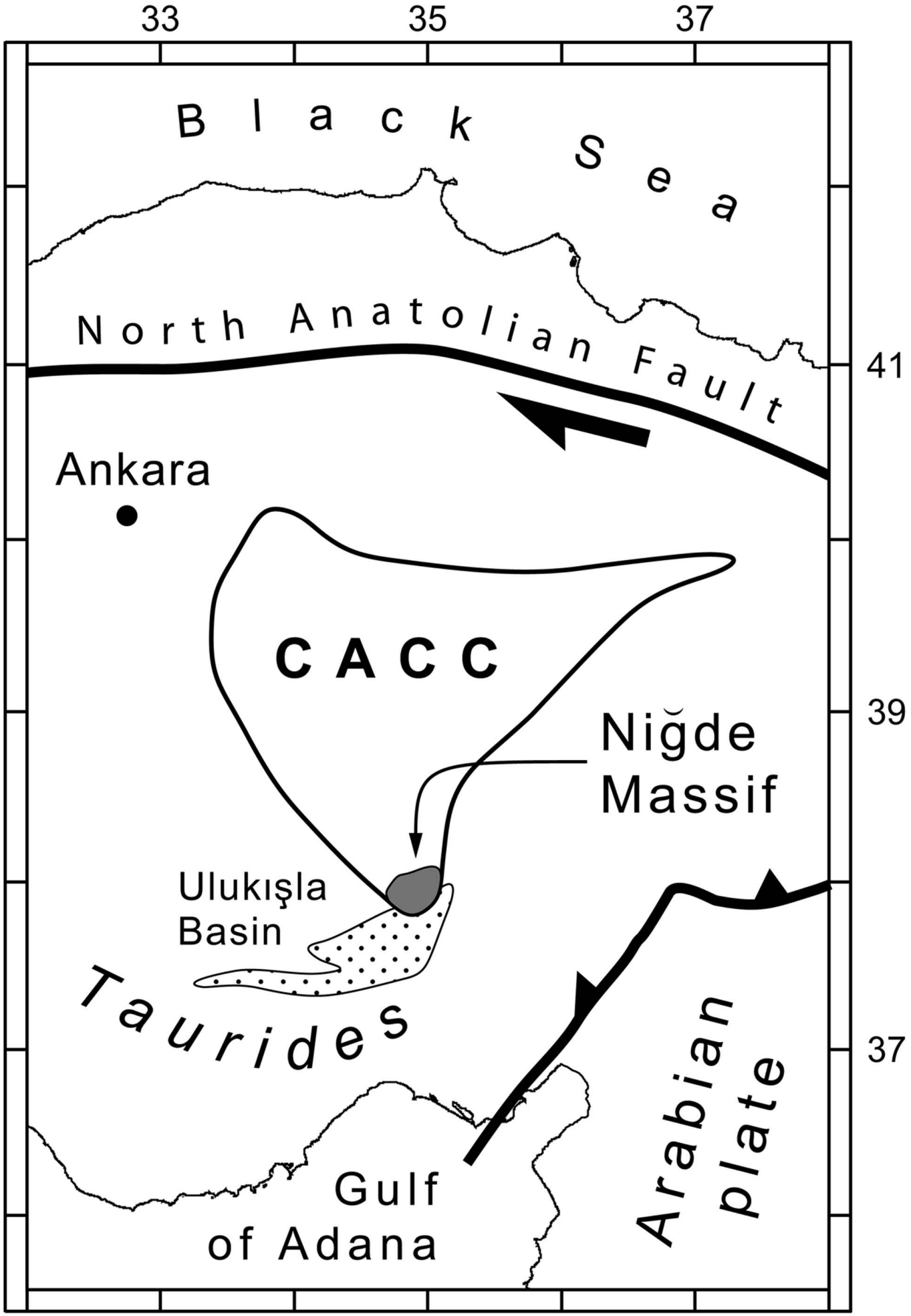
33
35
37
Black Sea
North Anatolian Fault
41
Ankara
CACC
39
Niğde
Massif
Ulukışla
Basin
Tauride s
37
Arabian
plate
Gulf
of Adana


Figure 3a
34.70°E
38.00°N
Gümüşler
95-22
N13
Figure 3b
Niğde
N16
N44
95-34
01-32
Fig.8a
Üçkapılı
N49
95-59
N67
N8
34.70°E
37.80°N
Kılavuz
Celaller
Çamardı
35.15°E
38.00°N
Kavlaktepe
Ecemiş
Fault
Zone
35.15°E
37.80°N
10 km
Lower unit
Üçkapılı-type granites
Southeastern slice of Gümüşler Fm
Aşıgediği Fm – mostly marbles with large inliers of metabasic rocks ('metamorphosed ophiolitic melange')
Eastern slice of Gümüşler Fm, with relictic migmatitic textures
Kaleboynu Fm
Gümüşler Fm, essentially migmatitic
Late Miocene to Quaternary sediments and volcanic rocks
Maastrichtian to Early Miocene sediments (until the Late Eocene, form the northern margin of Ulukışla basin)
Upper unit – massive ophiolite, mostly gabbros
Extensional detachment
Normal faults

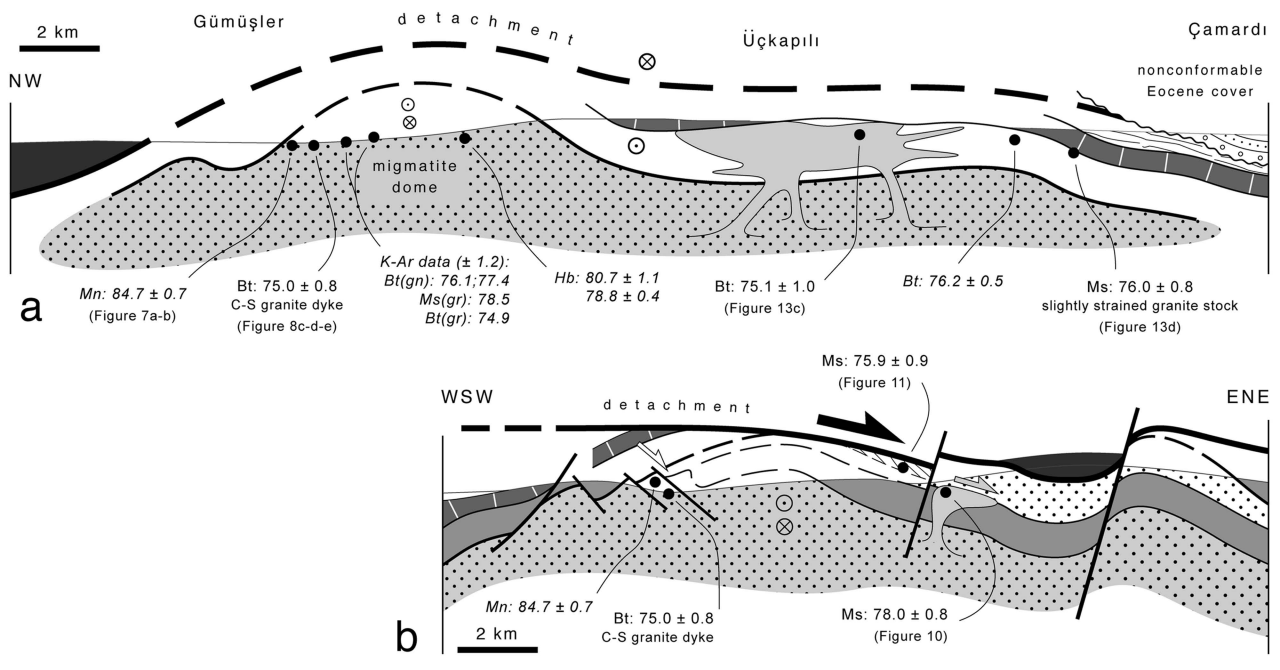
2 km
Gümüşler
detachment
Üçkapılı
Çamardı
NW
nonconformable
Eocene cover
migmatite
dome
Mn: 84.7 ± 0.7
(Figure 7a-b)
Bt: 75.0 ± 0.8
C-S granite dyke
(Figure 8c-d-e)
K-Ar data (± 1.2):
Bt(gn): 76.1;77.4
Ms(gr): 78.5
Bt(gr): 74.9
Hb: 80.7 ± 1.1
78.8 ± 0.4
Bt: 75.1 ± 1.0
(Figure 13c)
Bt: 76.2 ± 0.5
Ms: 76.0 ± 0.8
slightly strained granite stock
(Figure 13d)
a
Ms: 75.9 ± 0.9
(Figure 11)
WSW
detachment
ENE
Mn: 84.7 ± 0.7
Bt: 75.0 ± 0.8
C-S granite dyke
Ms: 78.0 ± 0.8
(Figure 10)
b
2 km

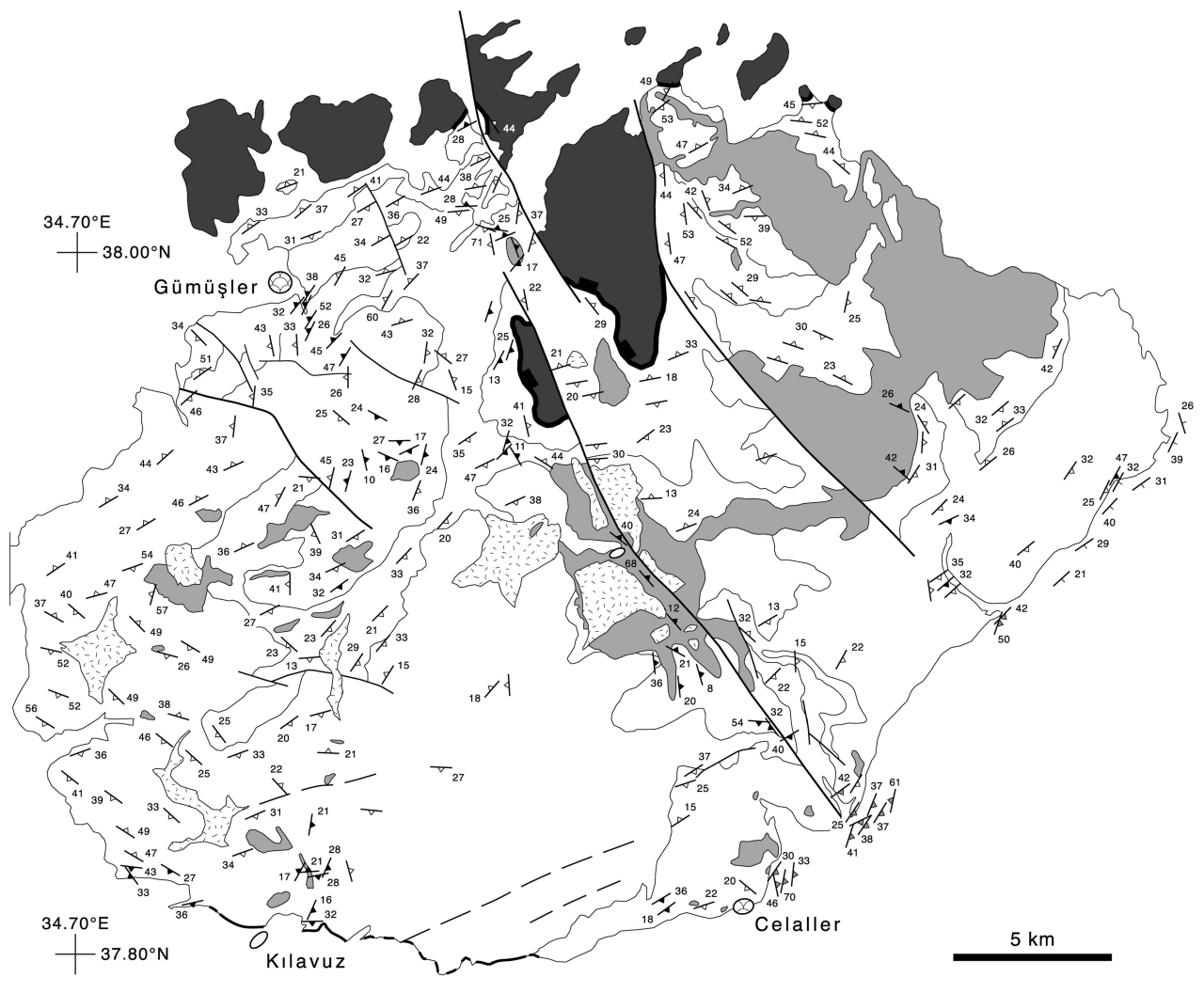

Stratification planes in nonconformable Oligocene sediments along the eastern margin of the massif, mainly after Göncüoğlu et al. (1991)

Schistosity planes in the pre-Oligocene sediments northeast of Celaller, after this work

Foliation planes in the Lower unit after Göncüoğlu et al. (1991) after this work


34.70°E
38.00°N
Gümüşler
Fig. 6
Fig. 9a
C-S
Fig. 10
Fig. 7a-b
C-S
Fig. 8c-d
Fig. 8b
Fig. 11
Fig. 7c-d-e
Fig. 9b
C-S
C-S
Fig. 12c
C-S
Fig. 12
d-e
34.70°E
37.80°N
31
40
18
20
22
34
48
Fig. 12a-b
Celaller
Çamardı
5 km
outcrops with a dense array of ultracataclastic joints
and/or massive ultracataclasites
striations and sense of shear on semi-brittle shear zones
at deeper levels of the Lower unit
Stretching lineations with/without shear sense determination
in metamorphic rocks
in granitoids,
with C-S fabric where indicated
22
grooves and striations, with plunge in degrees,
on the massif-bounding normal fault near Kılavuz
low-grade stretching lineations and sense of shear
in the pre-Oligocene sediments northeast of Celaller
areas showing abundant microbreccias
with ferric oxi-hydroxide mineralizations

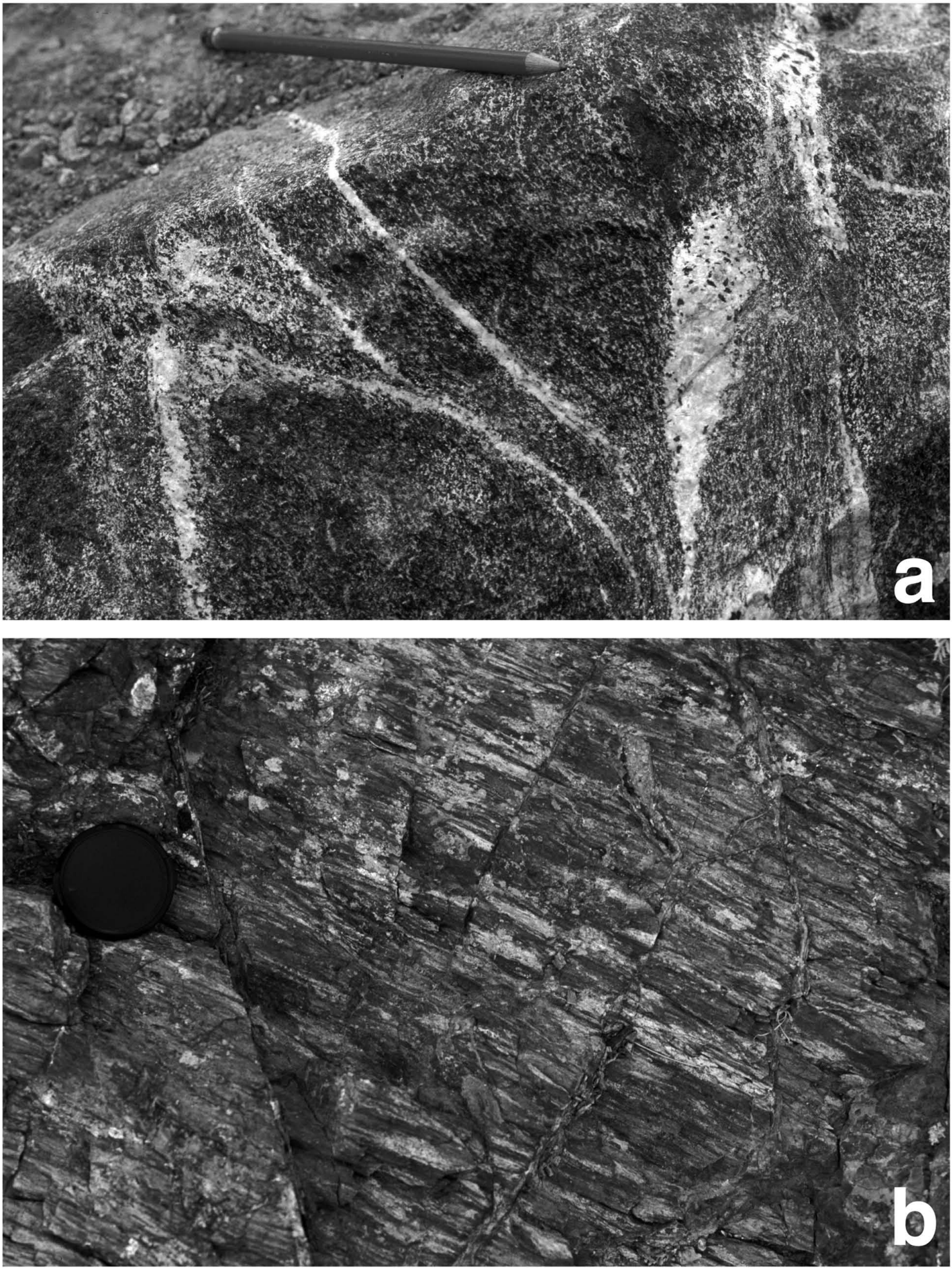
a
b

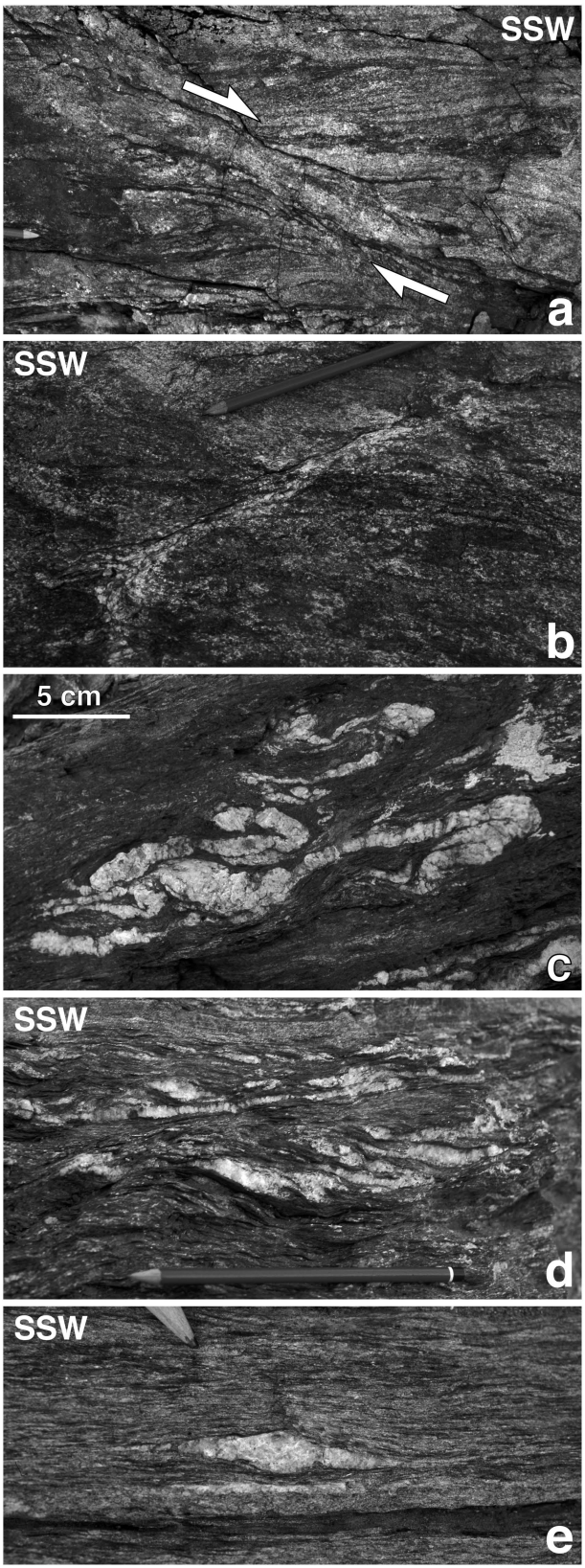
SSW
a
SSW
b
5 cm
c
SSW
d
SSW
e

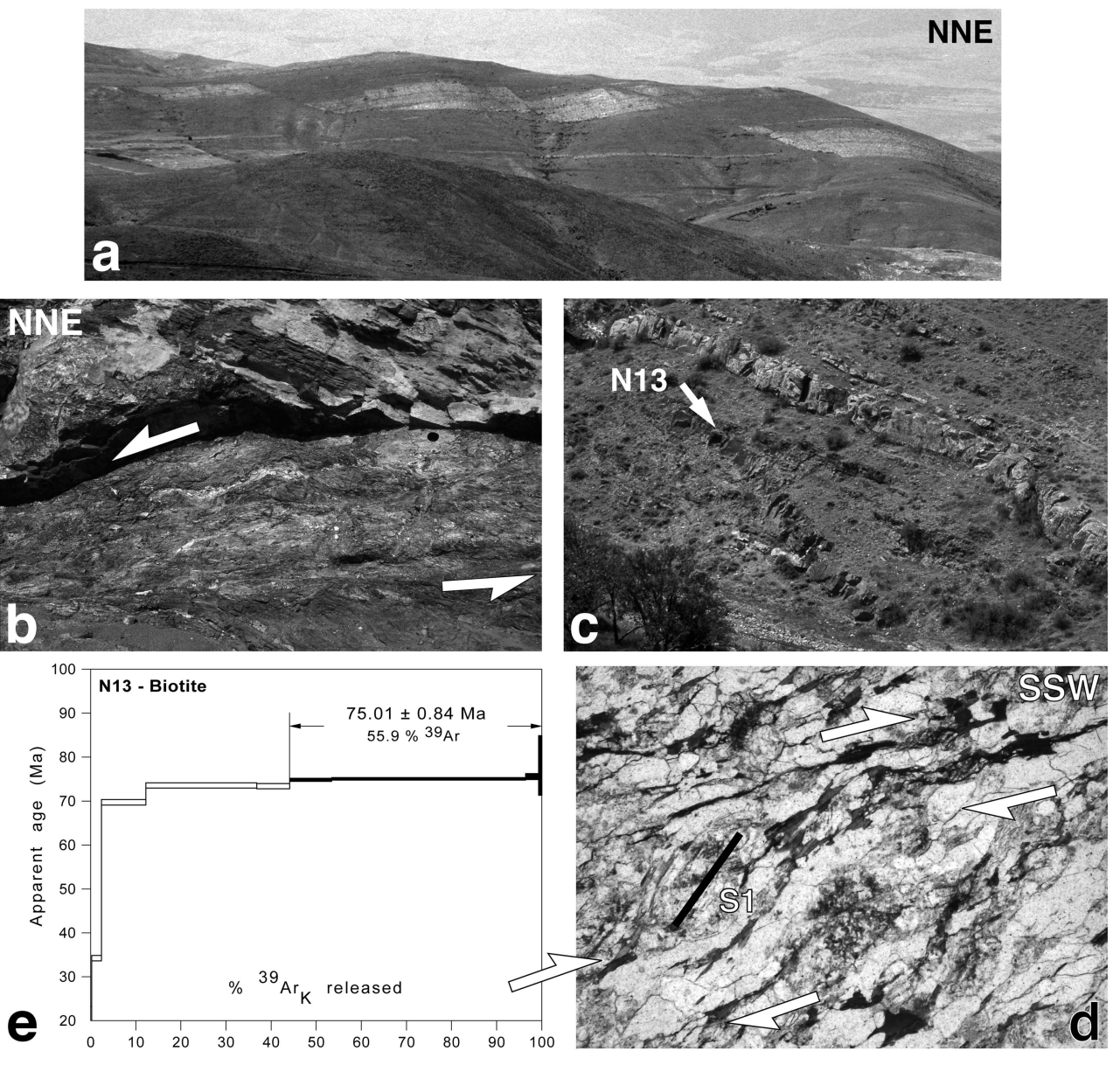
NNE
a
NNE
b
N13
c
N13 - Biotite
75.01 ± 0.84 Ma
55.9 % 39Ar
Apparent age (Ma)
% 39Ar K released
e
SSW
S1
d

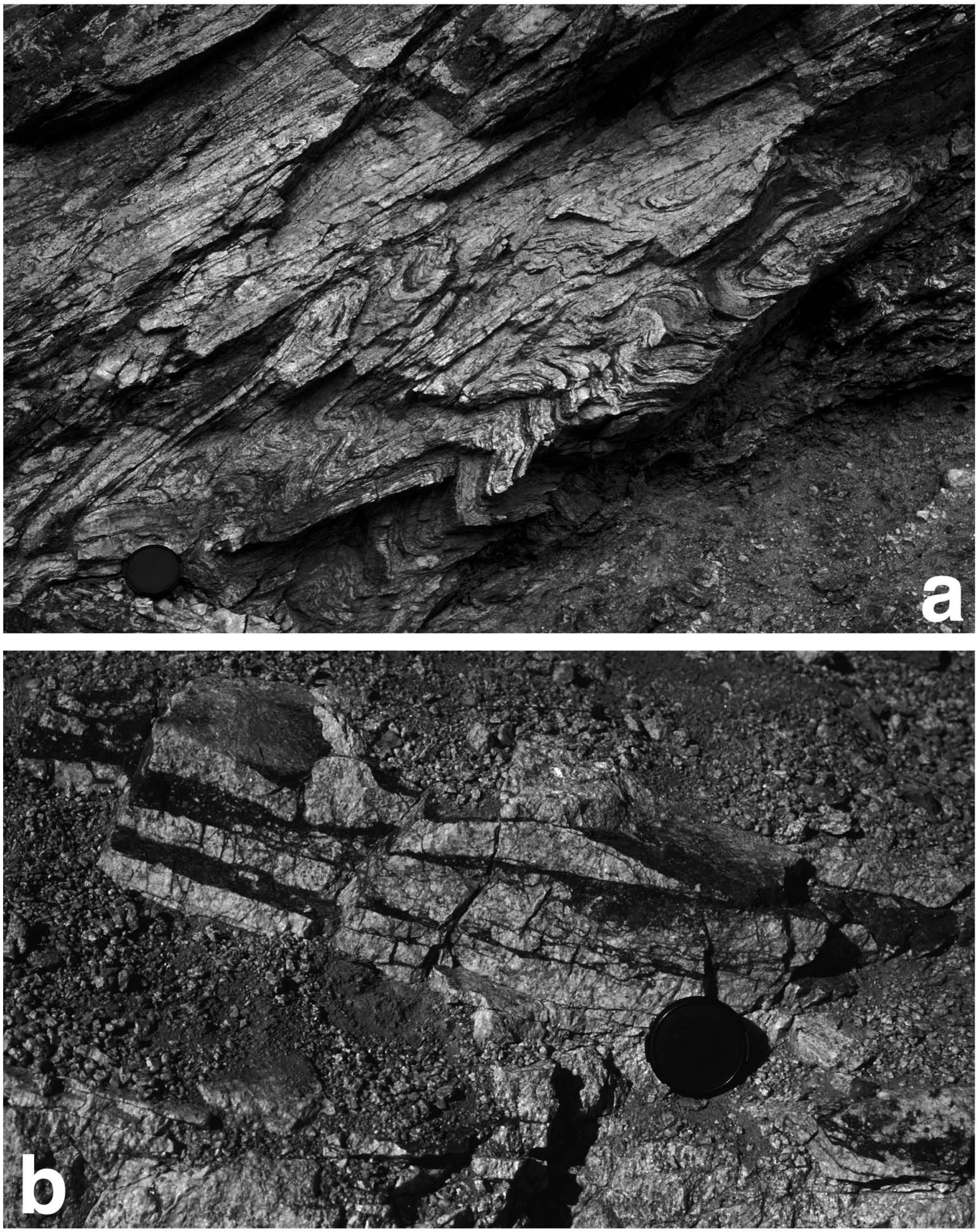
a
b

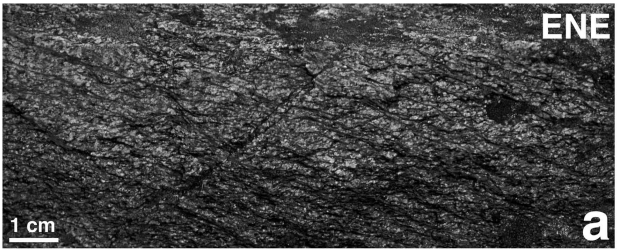
ENE
1 cm
a

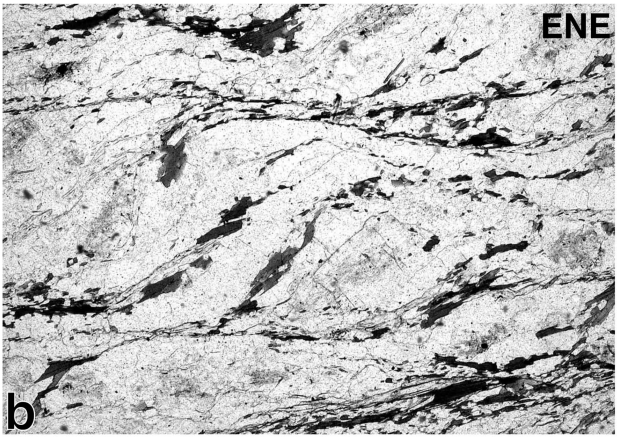
ENE
b

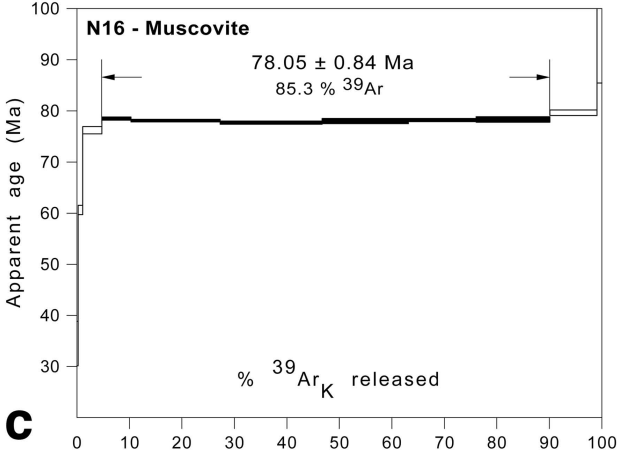
N16 - Muscovite
78.05 ± 0.84 Ma
85.3 % 39Ar
Apparent age (Ma)
100
90
80
70
60
50
40
30
% 39Ar K released
0
10
20
30
40
50
60
70
80
90
100
c

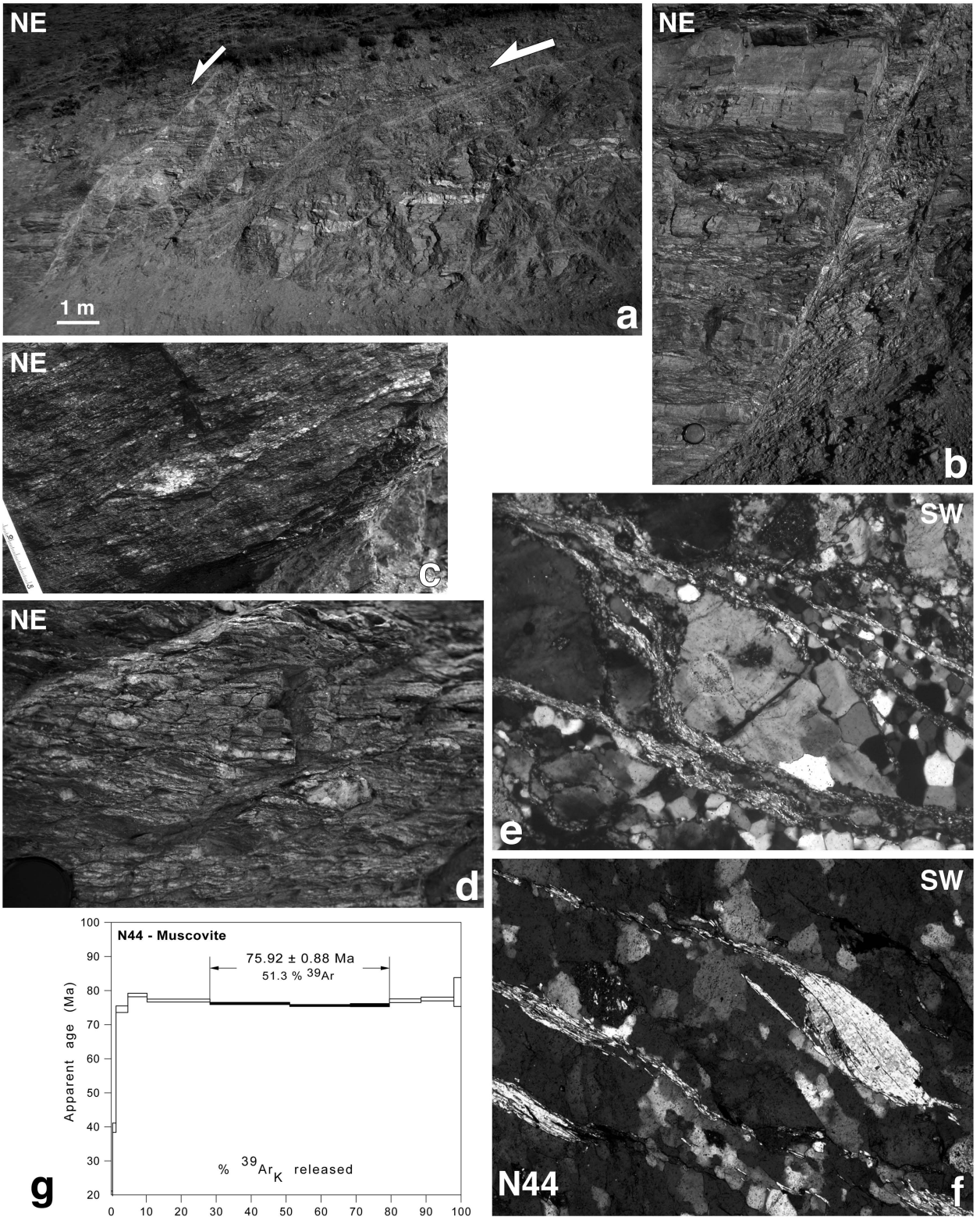
NE
1 m
a
NE
b
NE
c
NE
d
SW
e
SW
N44
f
N44 - Muscovite
75.92 ± 0.88 Ma
51.3 % 39Ar
Apparent age (Ma)
% 39Ar K released
g

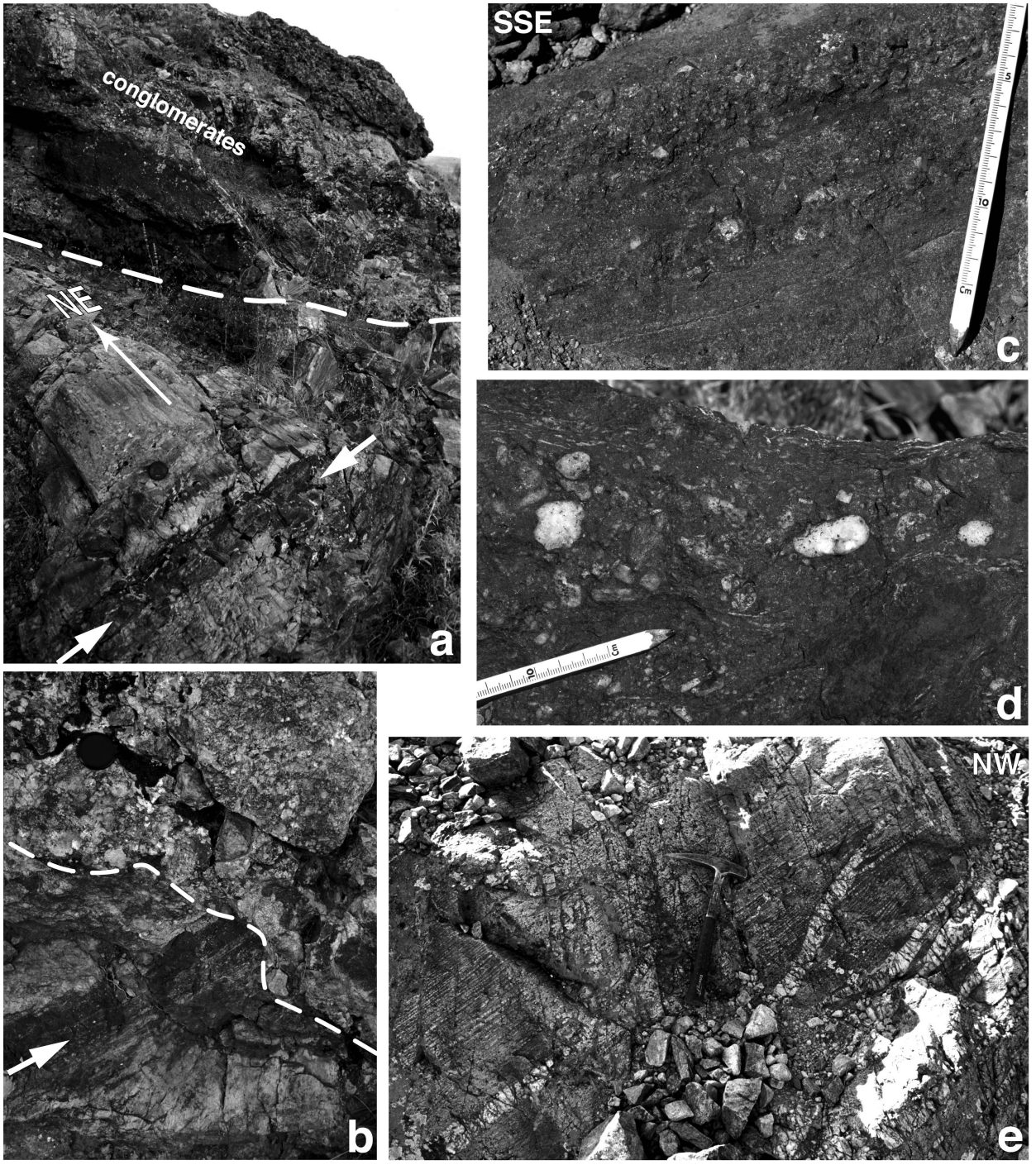
conglomerates
NE
a
SSE
c
d
b
NW
e

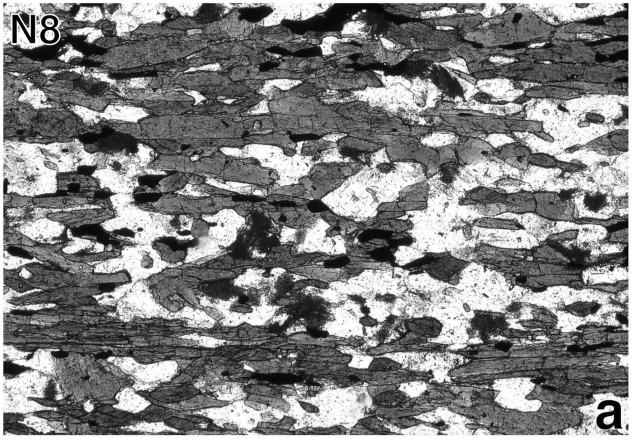
N8
a

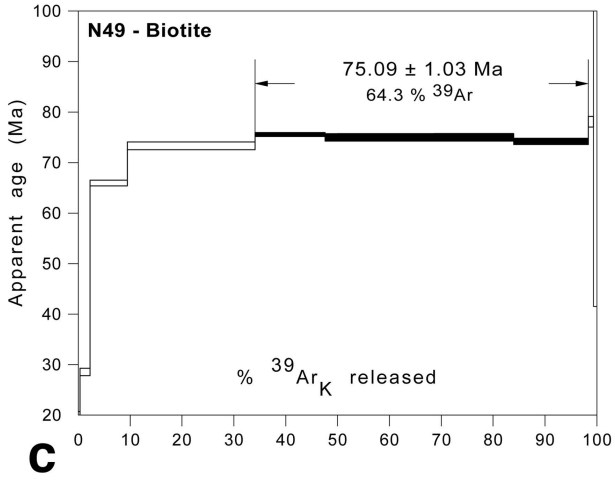
N49 - Biotite
75.09 ± 1.03 Ma
64.3 % 39Ar
Apparent age (Ma)
% 39ArK released
c

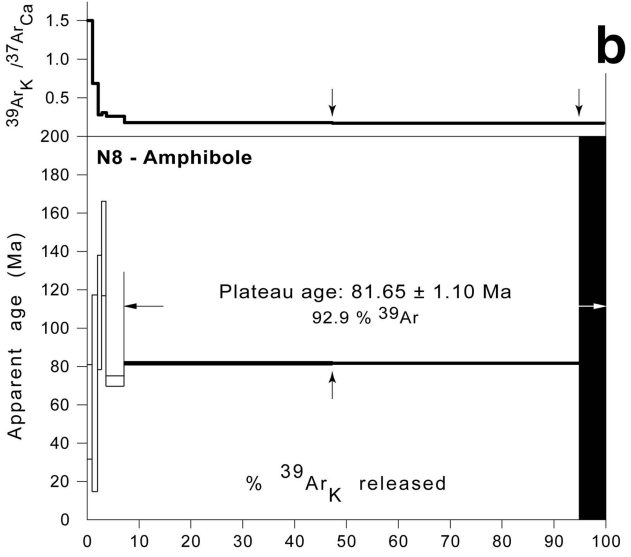
b
39ArK /37ArCa
N8 - Amphibole
Plateau age: 81.65 ± 1.10 Ma
92.9 % 39Ar
Apparent age (Ma)
% 39ArK released

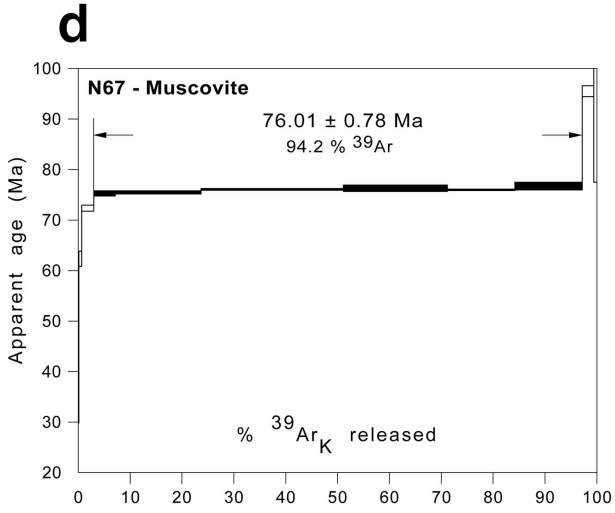
d
N67 - Muscovite
76.01 ± 0.78 Ma
94.2 % 39Ar
Apparent age (Ma)
% 39ArK released

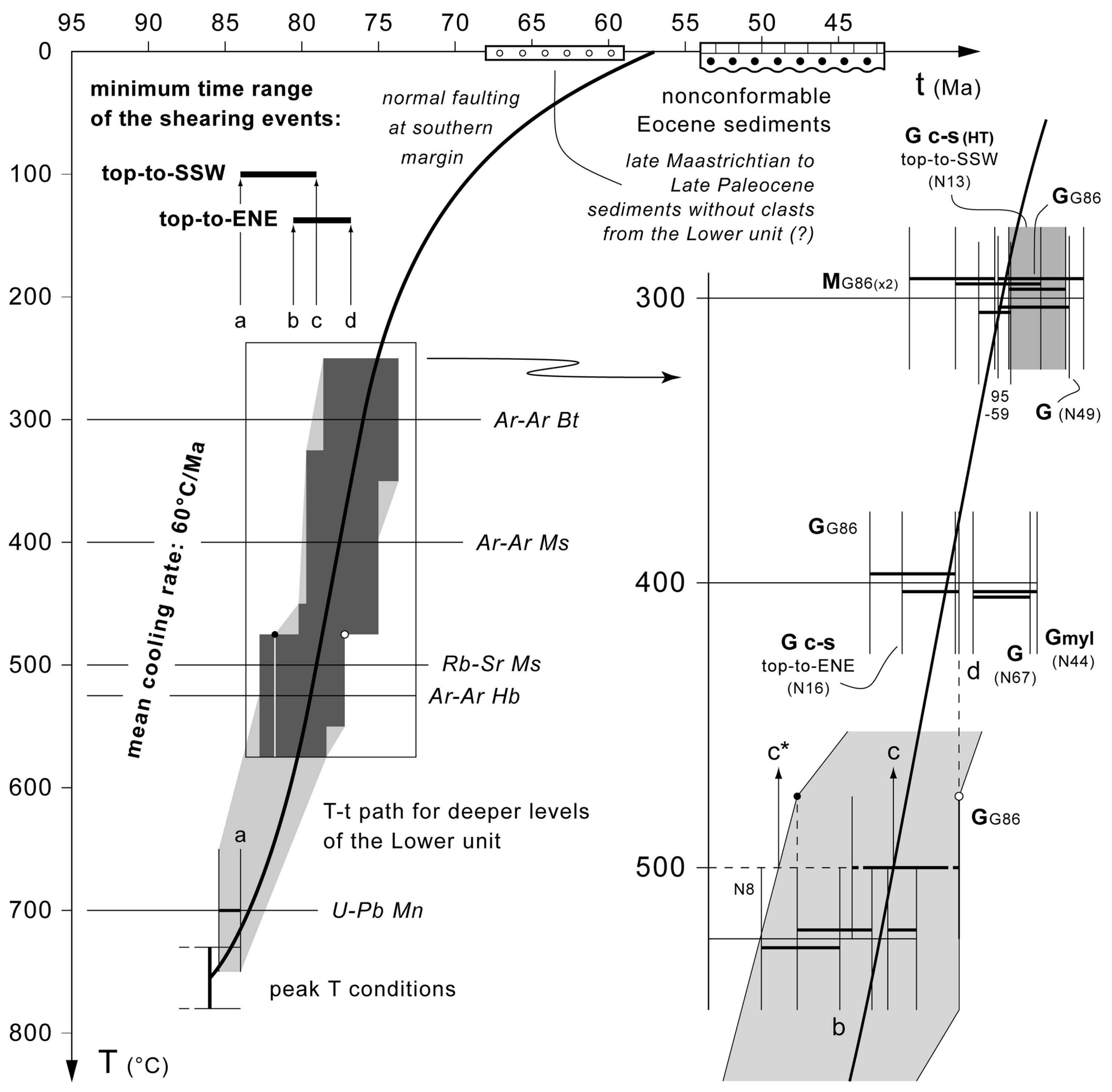
95
90
85
80
75
70
65
60
55
50
45
0
t (Ma)
minimum time range
of the shearing events:
top-to-SSW
top-to-ENE
a
b
c
d
normal faulting
at southern
margin
nonconformable
Eocene sediments
late Maastrichtian to
Late Paleocene
sediments without clasts
from the Lower unit (?)
100
200
300
400
500
600
700
800
Ar-Ar Bt
Ar-Ar Ms
Rb-Sr Ms
Ar-Ar Hb
U-Pb Mn
mean cooling rate: 60°C/Ma
T-t path for deeper levels
of the Lower unit
peak T conditions
T (°C)
G c-s (HT)
top-to-SSW
(N13)
GG86
MG86(x2)
95
-59
G (N49)
GG86
G c-s
top-to-ENE
(N16)
G
(N67)
Gmyl
(N44)
c*
c
GG86
N8
b

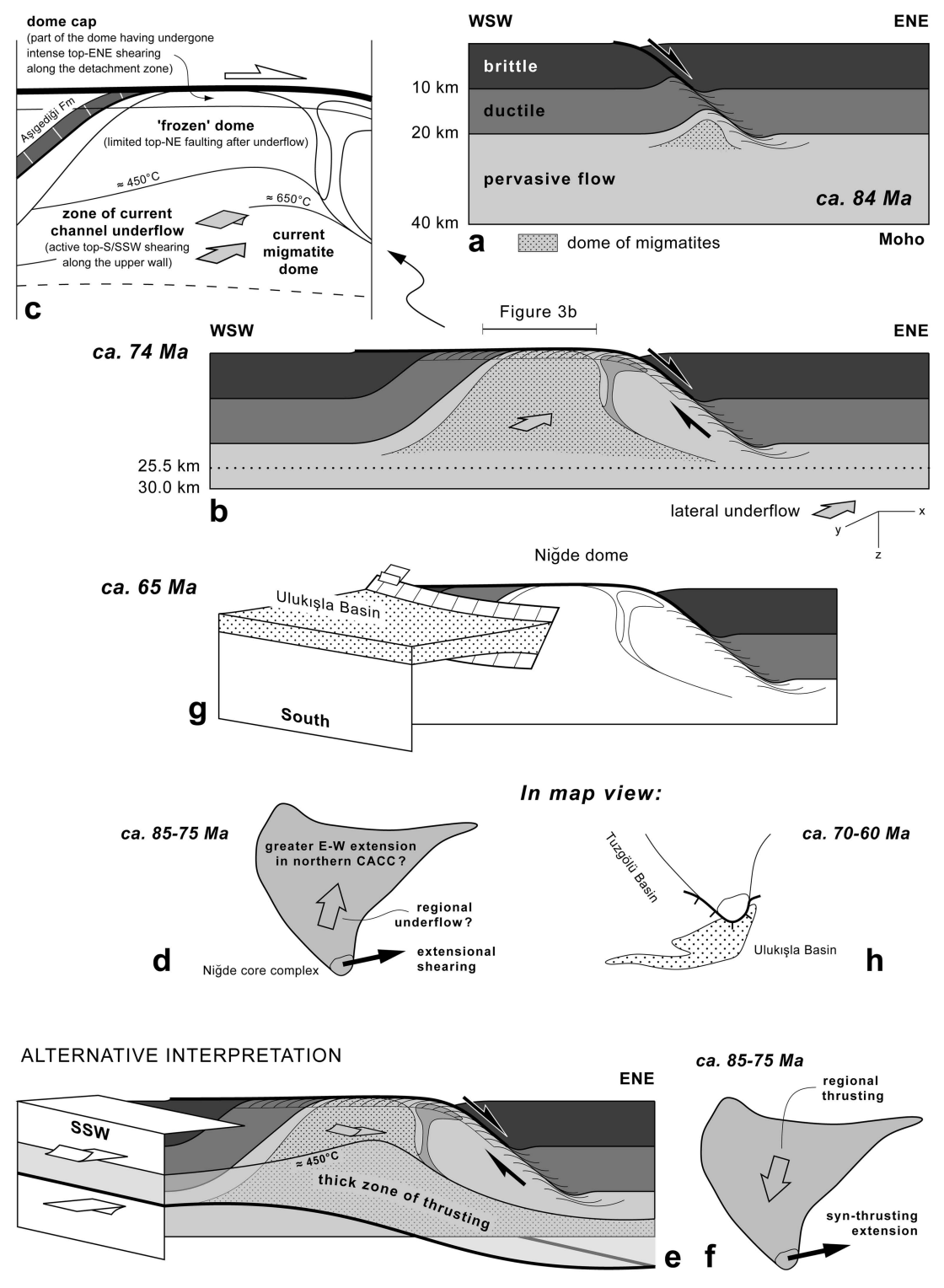
dome cap
(part of the dome having undergone intense top-ENE shearing along the detachment zone)
Aşıgediği Fm
'frozen' dome
(limited top-NE faulting after underflow)
≈ 450°C
≈ 650°C
zone of current channel underflow
(active top-S/SSW shearing along the upper wall)
current migmatite dome
c
WSW
ENE
brittle
ductile
pervasive flow
ca. 84 Ma
10 km
20 km
40 km
a
dome of migmatites
Moho
Figure 3b
ca. 74 Ma
WSW
ENE
25.5 km
30.0 km
b
lateral underflow
x
y
z
Niğde dome
ca. 65 Ma
Ulukışla Basin
South
g
In map view:
ca. 85-75 Ma
greater E-W extension in northern CACC?
regional underflow?
extensional shearing
Niğde core complex
d
ca. 70-60 Ma
Tuzgölü Basin
Ulukışla Basin
h
ALTERNATIVE INTERPRETATION
ENE
SSW
≈ 450°C
thick zone of thrusting
e
ca. 85-75 Ma
regional thrusting
syn-thrusting extension
f